STUDY OF BLAST WAVE IMPACT ON CONCRETE

by

AJIT GEEVARGHESE JOHN

Presented to the Faculty of the Graduate School of

The University of Texas at Arlington in Partial Fulfillment

Of the Requirements

For the Degree of

MASTER OF SCIENCE IN AEROSPACE ENGINEERING

THE UNIVERSITY OF TEXAS AT ARLINGTON

AUGUST 2005

ACKNOWLEDGEMENTS

I would like to express my deep gratitude and admiration to my advisor and mentor Dr. Frank K. Lu, who is a constant source of guidance and inspiration to me. I would also like to thank the other members of the committee, Dr. Seiichi Nomura and Dr. Donald R. Wilson, who have been extremely helpful during the whole process of thesis review and have helped enrich my thesis with their valuable suggestions. I would like to thank Mr. Rod Duke for helping me in my research work by utilizing his technical expertise with the lab equipment and also for all the extra efforts that he has taken on numerous occasions to run my experiments. I would also express my gratitude to Kenneth without whom I would have never been able to build the set up. I would also like to mention my special thanks to my colleagues in the lab - Philip, Satyanand, Noel and Dr. New who have gone out of their way many times to help me with the experimental work. A special thanks to Civilian Research Development Foundation (Grant No. RE2-2381-MO-02) – the initial sponsors of the project.

I would like to thank my roommates and my friends for all their encouragement especially Sapna, Ajit Sr., Ajay and Rahul and who have given me their help and moral support whenever I needed it. Most importantly I would like to thank my family who have been there for me always and are responsible for what I am today and without whom, the joy of completing the educational phase of my life would be incomplete.

June 27, 2005

ABSTRACT

STUDY OF BLAST WAVE IMPACT ON CONCRETE

Publication No. _____

Ajit Geevarghese John, M.S.

The University of Texas at Arlington, 2005

Supervising Professor: Dr. Frank K. Lu

The past decade has brought an upsurge of terrorist attacks throughout the world. A common form of attack is bombings employed against a civilian structure. These bombs lead to blast waves resulting from high explosive bursts in air, causing severe structural damage to buildings that often collapse before evacuation is possible. These blast waves subject the buildings to repeated dynamic loading in the form of reflecting shock waves which then finally lead to their destruction. Many studies have been carried out to understand the static loading of these structures. The current study is to protect existing buildings from an explosion. The proposal is to use a weak sand-cement mixture to form an outer boundary wall to absorb the impact of an explosion outside its boundary and protect the civilian structure.

A blast wave front possesses characteristics similar to a shock wave created in a shock tube and a reasonably realistic simulation of blast loading on structures can be made using an equivalent shock simulator. Such a shock simulator is safe, has high productivity and provides reproducible results. The set up is discussed in detail in this thesis.

While shock waves are different from blast waves in possessing a different profile, shock wave impacts still provide a reasonable simulation of the blast wave during an explosion. This is because the damage is caused by the impacting pressure. Smith and Hetherington (1994) discuss wave front parameters and scaling laws that can be used to simulate the effect of a charge of TNT at a certain distance from the target. These scaling laws can be used to compare the total pressure of the shock wave impact calculated based on the shock speed. Four strain gauges are mounted on a concrete cylinder specimen to detect the strength and time of the shock wave as it passes through the cylinder.

Studies show that the concrete mixture used can withstand shock wave impact at lower blast strengths (lower Mach numbers). At higher Mach numbers, the cylinder breaks off as a result of the stronger reflecting shock wave. A study of the wave propagation and attenuation trends in the cylinders is done in the thesis. There is also a comparison between the shock wave and blast wave strengths based on wave front and scaling parameters.

TABLE OF CONTENTS

LIST OF ILLUSTRATIONS

LIST OF TABLES

Table Page

CHAPTER 1

INTRODUCTION

The past decade has brought to the public attention terrorist bombings of civilian structures in many parts of the world. Much is being done in preventing such attacks by the concerned authorities. But there is also a need to protect our structures from such blasts. The issue of ensuring structural integrity from explosive blasts has been an active topic with the military and national security communities for years. Such concerns arose initially in response to bombing threats during World War II; however, they continued through the Cold War and, more recently, these concerns have grown with the increase in terrorism worldwide [1]. Thus there is an increasing need to find new methods to protect our buildings to save both civilians and property.

A bomb explosion can lead to extreme catastrophes in the vicinity of the blast. It leads to loss of life, severe damage to structures both internally and externally, and shutting down of vital support systems such as fire alarms, evacuation systems, ventilation etc. in the building. Loss of life is due to direct and indirect effects of the bomb blast. The direct effects are due to direct blast effects, debris impact, fire, and smoke. The indirect effects can be due to the inability to implement proper evacuations and provide timely medical aid as a result of inaccessibility.

The major impact of a terrorist-type bomb is blast effects, which will be discussed in detail now. Blast waves resulting from high explosive bursts in air can cause

severe structural damage to buildings that often collapse before evacuation is possible. Primary damage results from blast wave reflection when pressure is amplified through multiple reflections in multiphase media or in confined geometries. The development of a simulation facility for these impacts and their study are the objective of this research.

1.1 Blast and Shock waves

1.1.1 Definitions

When a condensed high explosive is initiated, the following sequence of events occurs. First, the explosion reaction generates hot gases of pressures ranging from 100 to 300 kilobars and temperatures of about 3000 to 4000 $^{\circ}$C. A violent explosion of these explosive gases then occurs and the surrounding air is forced out of the volume it occupies. As a result, a blast wave – a layer of compressed air – is formed in front of these gases containing most of the energy [2]. The major cause of all the destruction is the impact of this wavefront. This blast wave starts propagating out toward regions with lower pressure, i.e., atmospheric pressure. As the wave propagates, the pressure of the blast wavefront falls with increasing distance. This finally leads to cooling of the gases and a reversal of flow as a low-pressure region is created behind the front resulting in an equilibrium.

A shock wave is defined as a surface or sheet of discontinuity (i.e., of abrupt changes in conditions) whereby a marked increase in pressure, density, temperature and entropy is set up in a supersonic field or flow, through which the fluid undergoes a decrease in velocity. These severe gradients in pressure produce viscous effects and heat transfer i.e., non-equilibrium conditions, inside the shock [3].

1.1.2 Blast wave Simulator

The principles of shock wave propagation, reflection, diffraction and attenuation are well understood. In this study, we will use shock waves to simulate the impact of blast waves in explosions. Detonation of high explosive materials in free air creates a blast wave similar to the shock wave created by a shock tunnel. The basic difference between a shock wave and a blast wave is the pressures behind the wave. The pressures drop in the case of a blast wave is unlike a shock wave in which the pressure remains constant. This difference does not affect the impact pressures we are concerned in our study.

A high-performance shock tube was modified to accept a standard concrete test cylinder in its test section. The concrete cylinder is exposed to a shock wave. Shock strengths are varied to provide the desired equivalent blast wave parameters. Sensors are embedded in the concrete cylinder to study the propagation and attenuation of the wave in the cylinder. The knowledge gained can be useful in designing ordinary concrete structures for reducing the effects of terrorist-type bombs. The knowledge can also be used in accurate simulation of blast waves and their interactions.

1.2 Structure protection from blast waves

Protective strengthening and hardening are the two measures that can be taken to prevent or minimize damage to a structure from blast waves [1]. Most civilian structures are not "bomb proof," i.e., not much thought has been put into this aspect of structural design. The aim of both these measures is to increase the resistance of the structure to the applied loading. Strengthening can be defined as those measures taken to increase the

overall strength and stability of a structure under the specified loading. The objective of strengthening is to prevent a major structural failure, rather than reduction of damage to individual elements of the structure. Hardening is concerned with increasing the resistance of a structure or elements within it, to damage from impacting projectiles.

Strengthening of structures has to be done and thought during the design and construction phase of a structure. After a structure has been built it is usually not economically feasible to strengthen it by reinforcing it. The best way to protect an existing structure is hardening. A protective barrier built around an existing structure is one of the ways to harden the structure. In order to withstand the transient loads generated by bomb blasts, the elements of a structure need to be both massive and able to absorb large amounts of energy. For this reason, nearly all purpose-built protective structures are constructed of concrete.

A weak concrete mix (higher percentage of sand compared to cement) is being investigated for use as a protective dampening material. A secondary wall can be constructed using this mixture which will act as a sacrificial barrier to absorb large amounts of blast wave energy and thus absorbing the wave energy or reducing the effect of the blast wave impact. A weak mix is used as it can disintegrate into small particles that can absorb a large amount of energy in the process. The small particles in the debris tend to fly in different directions. Thus they will cause minimal damage to the existing structure compared to the larger size shrapnel emanating from the disintegration of a better concrete mix (lower percentage of sand). The proposed is also cost effective both in construction and cleanup after a blast.

1.3 Literature Review

The study of matter at extreme pressures was begun in the previous century and pioneered by Bridgman. A blast or shock wave impact on a structure comprises the dynamic loading. A structure subjected to dynamic loading cannot be tested easily since such tests are expensive and difficult to repeat. In the past, there has been development of explosive wave generators or high-speed gas guns in order to introduce shocks of precisely controlled amplitude and duration. A similar gas gun was developed by Bourne et al. [4, 5] to test plane and shear loading of materials. A projectile is shot at the target whose velocity is controlled using the pressure of the gun. Electromagnetic particle velocity measurement method for non-conducting or weakly conducting dense media was used to measure the shock propagation speeds through the target. A constant magnetic field is oriented parallel to the shock and perpendicular to the wire embedded parallel to the shock wave front. As the shock wave reaches the wire, it carries the wire along with its following flow, moving relative to the magnetic field at the particle velocity. The motion of the wire generates an electromotive force (which is measured) proportional to shock wave velocity.

There have been a few studies on the blast and projectile impact on concrete. Lepaanen [6] used spherical fragments to shoot against concrete blocks from various distances and at various speeds. Analyses of these structures were done to study both global and microscopic effects. It was found that greater damage occurred at the point of impact. This has been attributed to the fact that fragment impact causes only local damage whereas the blast wave impact causes global damage. Therefore, it is fair to assume that a shock wave impact has the same global effect as that of a blast wave

impact. Warren et al. [7] developed a numerical model for the penetration depths of projectiles impacting low-strength concrete. They found a 2-15% difference between the numerical model and the experimental data obtained. Certain effects such as dynamic fracture processes are very complex that are presently not well modeled.

There have been a few studies on the effect of shock waves on porous materials such as granular filters, screens and perforated plates, again primarily for infrastructure protection and blast mitigation. Bakken et al. [8] found that the shock wave impact due to pressurized air was higher than wave impact due to solid explosives of similar patterns. The attenuation of the shock wave is approximately same the same for waves generated by both methods. Therefore, the use of shock waves generated by a shock tube will result in an overestimate of the actual impact by a blast wave. Igra et al. [9] found that the use of porous materials leads to more interactions of the incident shock wave thereby reducing the impact pressure of the wave leaving the porous material. Based on the above works, a weak concrete mix (a material of high porosity) appears to be a good test material for a secondary barrier wall and simulating blast wave impact using shock waves seem to be suitable for blast wave mitigation.

CHAPTER 2

THEORETICAL BACKGROUND

The basic principle behind a shock tube has been exploited for over fifty years [14] for research that requires shock loading, high enthalpy or high speed flow, to list a few of the conditions that can be exploited. A shock wave is a strong discontinuity that imparts high pressure and temperature to the material behind it. If the disturbances in a compressible fluid are weak, they propagate at the speed of sound. When the cause of the disturbance is moving slower than the speed of sound, waves are developed which allow the fluid to redistribute itself to accommodate the disturbance. However, when a disturbance moves faster than the pressure waves it causes, fluid near the disturbance cannot react to it or "get out of the way" before it arrives. The properties of the fluid (density, pressure, temperature, velocity, etc.) thus change instantaneously as they adjust to the disturbance, creating thin disturbance waves called shock waves [10].

The one-dimensional equations for a constant area equilibrium flow with two regions (1 and 2) separated by a non-equilibrium region are [3]

$$\rho_1 u_1 = \rho_2 u_2 \tag{2-1a}$$

$$p_1 + \rho_1 u_1^2 = p_2 + \rho_2 u_2^2 \tag{2-1b}$$

$$h_1 + \frac{1}{2} u_1^2 = h_2 + \frac{1}{2} u_2^2 \tag{2-1c}$$

There are no restrictions on the size of the non-equilibrium region as long as there is a jump in the flow parameters across it. This non-equilibrium region may be idealized as a vanishing small region and the discontinuity is called a shock wave. Equations (2-1a)–(2.1c) are the general equations for a normal shock wave. The nonlinearity of the equations requires that they be solved numerically. Explicit solutions in terms of Mach number ahead of the shock M_1 can be obtained for a thermally and calorically perfect gas. Dividing (2-1b) by (2-1a) we get the following

$$u_1 - u_2 = \frac{p_2}{\rho_2 u_2} - \frac{p_1}{\rho_1 u_1} = \frac{a_2^2}{\gamma u_2} - \frac{a_1^2}{\gamma u_1} \tag{2-2}$$

Here the perfect gas relation for the speed of sound $a^2 = \gamma p/\rho$ has been used for arriving at the right-hand side. Using (2-1c) and some mathematical simplification we arrive at the following relation

$$u_1 u_2 = a^{*2} \tag{2-3}$$

Equation (2-3) is known as the Prandtl-Meyer relation. In terms of the Mach number $M^* = u/a^*$ we get

$$M_2^* = 1/M_1^* \tag{2-4}$$

We know that M^* is supersonic when M is supersonic and vice versa. Therefore the Prandtl relation shows that the velocity change across a normal shock must be from supersonic to subsonic or vice versa. In other words, the equations thus far allow for either a compression or an expansion process across the discontinuity. However, there is a dissipation effect across a shock wave as a result of which there can be only a decrease of velocity. This distinction can be obtained by appealing to the second law of thermodynamics. The relation between M^* and M is [3]

$$M^{*2} = \frac{(\gamma+1)M^2}{(\gamma-1)M^2+2} \qquad (2\text{-}5)$$

Using equations (2-3), (2-4) and (2-5) in (2-1), we arrive at the following equation for the pressure jump across a shock wave

$$\frac{p_2 - p_1}{p_1} = \frac{\Delta p_1}{p_1} = \frac{2\gamma}{\gamma+1}(M_1^2 - 1) \qquad (2\text{-}6)$$

The ratio $\Delta p_1 / p_1$ is defined as the shock strength. The pressure ratio across a shock wave may also be written as

$$\frac{p_2}{p_1} = 1 + \frac{2\gamma}{\gamma+1}(M_1^2 - 1) \qquad (2\text{-}7)$$

The above ratio is manipulated indirectly to produce the shock wave of the required Mach number.

2.1 Propagating Shock wave

In the above discussion, we assumed that the shock wave is stationary and the fluid is moving at a speed u_1. Alternatively let us assume that the fluid is stationary ahead of the shock wave at a speed of

$$c_s = u_1 \qquad (2\text{-}8)$$

The fluid behind the wave is therefore following with the speed

$$u_p = u_1 - u_2 = c_s(1 - u_2/u_1) \qquad (2\text{-}9)$$

The Mach number of the shock wave $M_1 = c_s / a$ is used in equation (2-7) to obtain

$$c_s = a_1\left(\frac{\gamma-1}{2\gamma}+\frac{\gamma+1}{2\gamma}\frac{p_2}{p_1}\right)^{1/2} \tag{2-10}$$

The Rankine-Hugoniot relations for density and temperature ratios are [3]

$$\frac{\rho_2}{\rho_1}=\frac{1+\frac{\gamma+1}{\gamma-1}\frac{p_2}{p_1}}{\frac{\gamma+1}{\gamma-1}+\frac{p_2}{p_1}}=\frac{u_2}{u_1} \tag{2-11}$$

$$\frac{T_2}{T_1}=\frac{p_2}{p_1}\frac{\frac{\gamma+1}{\gamma-1}+\frac{p_2}{p_1}}{1+\frac{\gamma+1}{\gamma-1}\frac{p_2}{p_1}} \tag{2-12}$$

Substituting (2-10) and (2-12) in (2-9) we obtain the fluid velocity in terms of the shock strength

$$u_p=\frac{a_1}{\gamma}\left(\frac{p_2}{p_1}-1\right)\left\{\frac{\frac{2\gamma}{\gamma+1}}{\frac{\gamma-1}{\gamma+1}+\frac{p_2}{p_1}}\right\}^{1/2} \tag{2-13}$$

The above equation relates the flow speed to the shock strength.

2.2 Shock tube

A shock tube basically consists of two sections – a driver tube and a driven tube. A pressure difference initially exists between the two sections. High pressure in the driver section and low pressure in the driven section are separated by a diaphragm as shown in Fig. 3.1. The diaphragm is ruptured, creating a contact surface (slip surface) between the

high and low pressure (Fig. 3.2). A normal one-dimensional shock wave arises from the pressure discontinuity and propagates into the driven section at Mach number M_s.

One-dimensional wave theory is used to obtain the resulting shock wave properties and flow conditions. The primary parameter concerning shock wave properties is the initial driver-to-driven pressure ratio p_4/p_1. The pressure ratio p_2/p_1 across the shock wave is related to the p_4/p_1 by the basic shock tube equation (Equation 2-17).

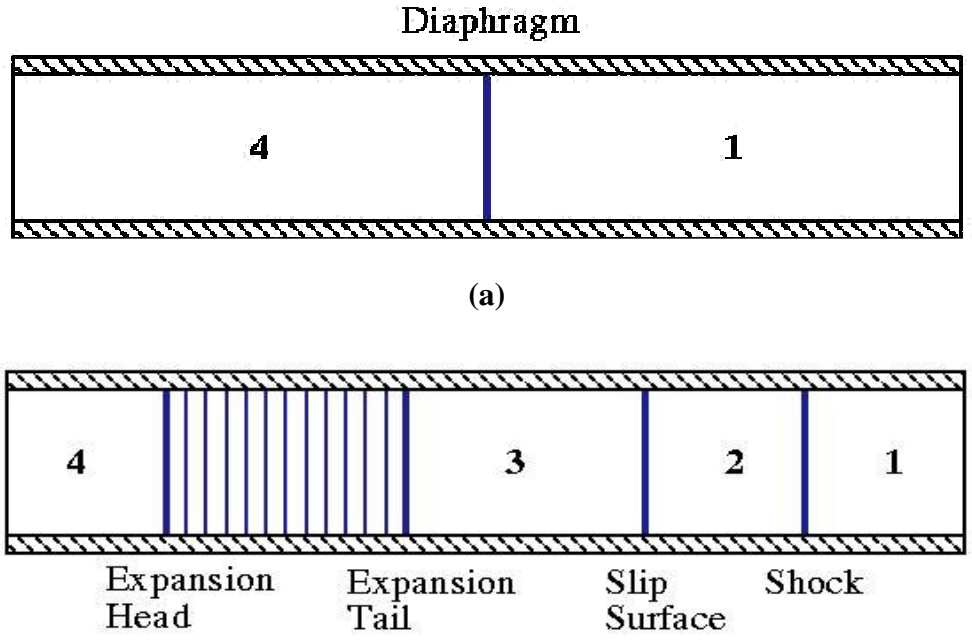

Figure 2.1 Schematic of shock tube process. (a) before and (b) after the rupture of the diaphragm.

At the initial instant when the diaphragm is burst, the pressure distribution is ideally a step function. The high pressure propagates into the driven tube as a shock wave with a speed c_s, while an unsteady expansion wave propagates into the driven tube with the speed a_4 at its front (Fig. 3.3). The condition of the fluid is denoted by (2) and that of

the fluid traversed by the expansion wave is denoted by (3). The interface between regions 2 and 3 is called the contact surface or slip surface. It is the same boundary between the fluids as the diaphragm before it was burst. The temperatures and densities across the contact surface may be different but continuity conditions require that the pressures and velocities are the same:

$$p_2 = p_3 \tag{2-14}$$

$$u_2 = u_3 \tag{2-15}$$

In the above equation, u_2 is given by (2-13) and the expansion wave u_3 is given by [3]

$$u_3 = \frac{2a_4}{\gamma_4 - 1}\left[1 - \left(\frac{p_3}{p_4}\right)^{\frac{\gamma_4 - 1}{2\gamma_4}}\right] \tag{2-16}$$

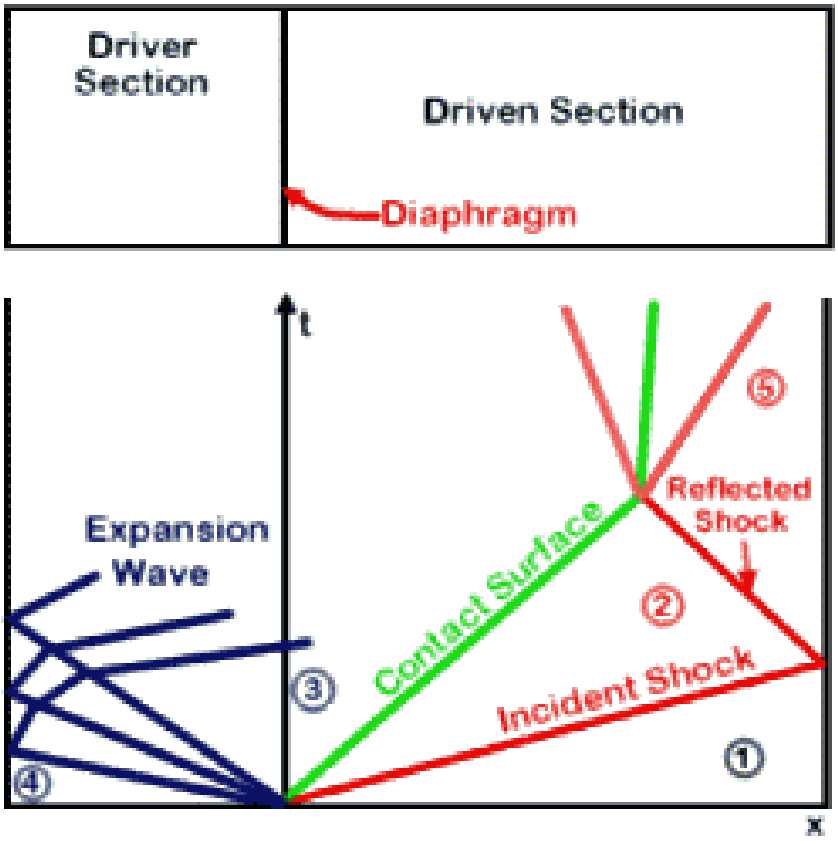

Figure 2.2 Motion in a shock tube represented by a x-t diagram. [11]

Equating (2-13) and (2-16) and substitution of (2-14) results in the basic shock tube equation

$$\frac{p_4}{p_1} = \frac{p_2}{p_1}\left[1 - \frac{(\gamma_4 - 1)(a_1/a_4)(p_2/p_1 - 1)}{\sqrt{2\gamma_1}\sqrt{2\gamma_1 + (\gamma_1 + 1)(p_2/p_1 - 1)}}\right]^{\frac{-2\gamma_4}{\gamma_4 - 1}} \qquad (2\text{-}17)$$

This equation implicitly gives us the shock strength as a function of the diaphragm pressure ratio p_4/p_1.

The Mach number M_s of the incident shock wave from (2-7) is given by

$$M_s = \sqrt{\frac{2\gamma_1}{\gamma_1 + 1}\left(\frac{p_2}{p_1} - 1\right) + 1} \tag{2-18}$$

The total pressure p_o of the flow behind the shock wave based on the isentropic relations is given by

$$p_o = p_2\left(1 + \frac{\gamma_1 - 1}{2} M_s^2\right)^{\frac{\gamma_1}{\gamma_1 - 1}} \tag{2-19}$$

For the present study, this pressure is the impact pressure of the wave on the concrete cylinder.

Equation (2-17) can be solved only numerically and therefore not very accurate. Experimentally, a time-of-flight method can be used for obtaining the Mach number of the shock wave from measurements. The shock Mach number can be obtained by

$$M_s = \frac{d}{t_{PT2} - t_{PT1}} (\gamma R T_1)^{-1/2} \tag{2-20}$$

where t_{PT2} and t_{PT1} are arrival times at two transducers in the path of the shock flow, d is the distance between them, γ is the ratio of specific heats for the gas, R is the gas constant for gas, and T_1 is temperature of gas in the driven tube.

2.3 Blast wavefront parameters

When high explosive materials are detonated, very high local pressures are created. In the idealized description of a point blast in an infinite domain, the sudden point pressure disturbance develops into a spherical shock wave. A blast wavefront, far from the point, possesses characteristics similar to a one-dimensional shock wave created

by a shock tube. Both waves display a discontinuous increase in pressure which propagates at supersonic velocity. However, pressure-time profiles following the waves are different. Behind a blast wave, the static pressure steadily decreases. In a one-dimensional shock front generated in a shock tube, the static pressure remains steady until the arrival of waves reflected off the closed end of the driver tube.

Smith and Hetherington [2] discuss wavefront parameters and scaling laws to relate blast waves from explosives and shock waves generated in shock tubes. Each simulation is equivalent to an explosion of a particular strength at a particular distance. The wavefront static pressure P_2 is given by

$$P_2 = 101.325 + \frac{1407.2}{Z} + \frac{554}{Z^2} - \frac{35.7}{Z^3} + \frac{0.625}{Z^4} kPa \quad (0.05 \le Z \le 0.3) \quad \text{(2-21a)}$$

$$P_2 = 101.325 + \frac{619.4}{Z} - \frac{32.6}{Z^2} - \frac{213.2}{Z^3} kPa \quad (0.3 \le Z \le 1) \quad \text{(2-21b)}$$

$$P_2 = 101.325 + \frac{66.2}{Z} + \frac{405}{Z^2} + \frac{328.8}{Z^3} kPa \quad (1 \le Z \le 10) \quad \text{(2-21c)}$$

The scaled distance parameter Z is given by

$$Z = \frac{R}{W^{1/3}} \quad \text{(2-22d)}$$

where R is the distance from the charge center in meters and W is the charge mass in kilograms of TNT. With the Z parameter, an equivalent blast strength and range is determined for each test in the shock tube.

The dynamic pressure q_2 of the wavefront is given by [2]

$$q_2 = \frac{5P_2^2}{2(P_2 + 7P_{amb})} \quad \text{(2-23)}$$

where P_{amb} is the ambient pressure and is equal to 101.325 kPa.

The total pressure of the blast wavefront can be obtained from the addition of the results of (2-23) and (2-22) and compared with the total pressure of the shock wave obtained in equation (2-19). The detailed studies are done in Chapter 4.

CHAPTER 3

EXPERIMENTAL SETUP

The blast wave simulator is basically a non-reflecting shock tube in which a concrete test specimen is directly exposed to a shock wave. The other major components of the simulation are the concrete cylinder and the data acquisition system. Each of these shall be described in detail in the following sections.

3.1 Shock tube

The main components include a driver tube, driven tube, expansion nozzle, test section and vacuum tank as shown in Fig 3.1

3.1.1 Driver and Driven tubes

The shock tube consists of a driver tube segment and three driven tube segments. The four segments have been designed for a maximum operating driver pressure of 41.4 MPa (6000 psi) and they were hydrostatically tested to 62.1 MPa (9000 psi) [13]. The driver tube is 3 m (10 ft) long and has an internal diameter of 15.24 cm (6 in.) and an external diameter of 20.32 cm (8 in.). One end is closed off with a hemispherical end cap and the other end has a 48.26 cm (19 in.) diameter, 11.43 cm (4.5 in.) thick flange which allows the driver to be bolted to the diaphragm section and the driven tube.

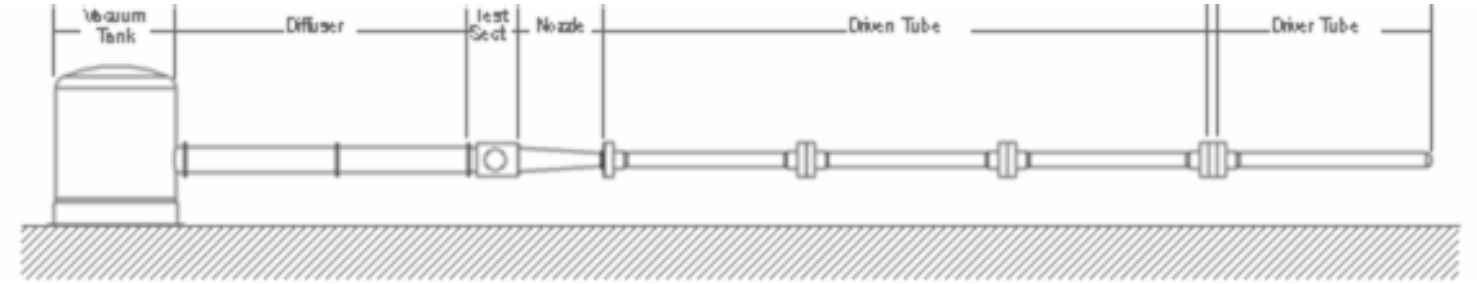

Figure 3.1 Components of the facility.

The various sections of the shock tube are bolted together by 5.08 cm (2 in.) diameter bolts. The flanges at each of the section joints are held together by eight of these bolts. The flanges have a double O-ring groove machined in them for sealing purposes. Both high pressure and vacuum seals are obtained by these O-rings.

The driven tube is constructed of three segments of 2.74 m (9 ft) length each. All these segments have a flange at each end identical to the one on the driver section. Each of the driven tube sections have the same dimensions as of the driver tube resulting in a driver-to-driven tube area ratio of one. The driven tubes can be vacuumed to absolute pressure as low as 3.4 kPa (0.5 psi). Between the driver and driven tubes lies an intermediate tube section 11.4 cm (4.5 in.) long. The intermediate section pressure is initially held at half the driver section pressure. Thin diaphragms, usually of metal such as aluminum or steel, separate the three sections, as shown in Fig. 3.2.

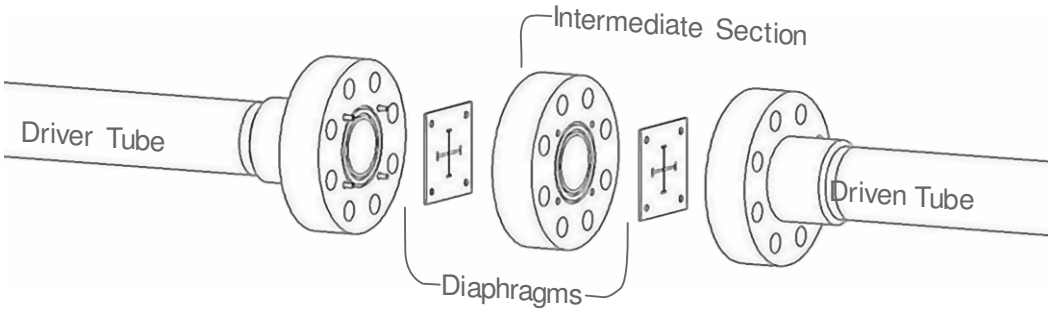

Figure 3.2 Exploded view of diaphragm section shows the driver section diaphragm(left) and intermediate section diaphragm(right).

Decreasing the intermediate section pressure causes the driver section diaphragm to rupture, which is immediately followed by the rupture of the intermediate section diaphragm. A strong shock wave is generated by the sudden large pressure difference. The shock wave propagates into the low pressure (driven) section at supersonic velocity. This process is shown in Fig. 3.3.

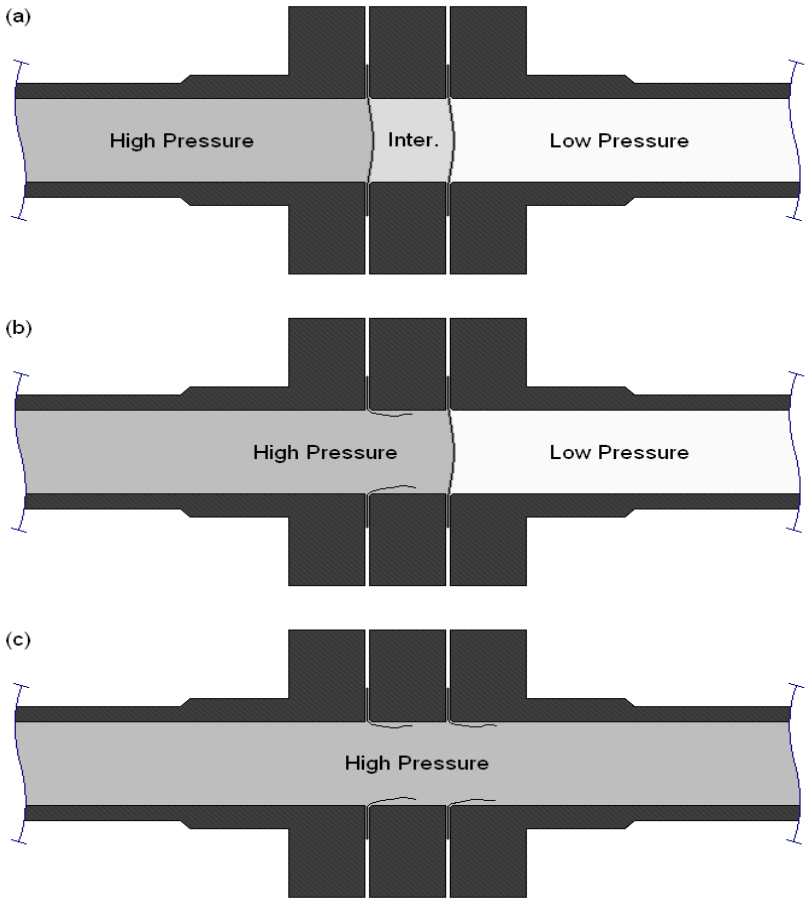

Figure 3.3 The diaphragm rupture process: (a) Three initial separate regions (b) decrease in intermediate pressure section leading to an increase in pressure difference across driver diaphragm and finally its rupture (c) the ensuing rupture causes an equal pressure difference across the intermediate diaphragm and its rupture.

A pressure transducer placed at 260.8 cm (8.5 ft) from the secondary diaphragm on the first driven tube provides the trigger signal for the data acquisition system. The two pressure transducers used to capture the time instants of the shock wave propagating in the driven tube are placed at a distance of 137.2 cm (54 inches) on the driven tube. The first pressure transducer used to capture the time instant of shock wave propagation is placed at a distance of 83.8 cm (33 inches) from the trigger transducer on the driven tube.

3.1.2 Nozzle, Test Section and Vacuum Tank

The end of the driven tube connects to an expansion nozzle, increasing cross-sectional diameter from 15.2 cm (6 in.) to 30.5 cm (12 in.) along a distance of 117cm (46 in.). The nozzle is a conical design with a 7.5 degree half-angle expansion. The shock wave propagates through the driven tube at a given Mach number until it encounters the nozzle through which the flow is isentropically expanded causing the Mach number to increase while the total pressure is conserved. Therefore the shock wave total pressure in the test section is the same as the total pressure in the driven tube. The nozzle was designed for operation at Mach numbers between 5 and 16 if the facility is configured as a shock tunnel.

The test section is a semi-free jet design with two access ports on either side. The test section is 55.9 cm (22 in.) long and the circular access ports on either side are 23 cm (9 in.) in diameter and can be used for optical windows if desired. The test section houses a conical converging section at the rear, leading to the diffuser. Flow exiting the diffuser continues into a vacuum tank. The vacuum tank has volume of 4.25 m^3 (150 ft^3), a diameter of 1.68 m (66 in.), and a height of 2.13 m (84 in.) with torospherical caps on the top and bottom to save weight. This vacuum tank has a 50.8 cm (20 in.) manhole to allow

access for cleaning or retrieving debris that was blown down during a test. A 35.6 cm (14 in.) vacuum pipe is connected to the tank by a flange joint with a double O-ring seal. This pipe is connected to the diffuser. The tank is equipped with a high flow rate check valve for automatic pressure relief. There is also a pipe collar which is used as a manual vent valve at the end of the test. The vacuum tank was designed for a pressure rating of 103 kPa (15 psi) vacuum and 551 kPa (80 psi) internal pressure. It has been proof tested to an internal pressure of 827 kPa (120 psi).

3.1.3 Other systems

The entire shock tube is supported and anchored to prevent any movement while firing the tube. The driver tubes are mounted on thrust stands with rollers for ease of movement and changing diaphragms. A pneumatic pump is used to move the tubes on the rollers. The vacuum pump is connected to the vacuum tank.

3.2 Instrumentation

3.2.1 Data Acquisition System

Data is acquired using a system manufactured by DSP Technologies. It consists of a Traq I 4012P system controller, 5204 memory module, six 2812 digitizers, six 1008 amplifiers, two 2860 digitizers, and 5005 memory module. The system is capable of simultaneously collecting 12-bit samples from 48 channels at 100 kHz and 8 channels at 1 MHz. Samples from 100 kHz channels are passed to the 5204 memory module while samples from 1 MHz channels are passed to the 5005 memory module, with storage capacities of 512 K samples and 2048 K samples, respectively (where K=1024). The available time frame for data acquisition is limited by memory module capacity and

inversely proportional to the number of active channels. For 100 kHz samples (the sampling rate used in the experiments), the time frame is given by

$$t_{100k} = \frac{512(1024)}{(100kHz)(n_k)}$$

where n_k is the number of active 100 kHz channels.

A cycle of writing and overwriting new data into memory continues until an external trigger signal is received. After the trigger signal is received, memory continues to be overwritten for a preset duration of time. Therefore, data acquired may be pre- or post-trigger. The trigger signal is supplied by an external home-made circuit which monitors the voltage from a PCB pressure transducer mounted in the driven tube. The circuit provides a step input signal to the data acquisition system when the transducer reaches a voltage level predetermined to be evidence of a shock wave.

A host computer is located inside the laboratory control room approximately 12.2 m (40 ft) from the test section. Data is transferred to a host computer via a National Instruments GPIB 110 bus extender. The host computer is used for data acquisition system setup as well as for data reduction and analysis.

3.2.2 Instrumentation

The facility is instrumented with several types of pressure transducers. Three PCB dynamic pressure transducers (PCB model111A24) are flush-mounted in the driven tube. Two are used to obtain shock wave static pressures and times of arrival. The third serves as an external trigger signal to the data acquisition system. These transducers have a full scale pressure rating of 10 kpsi, a resolution of 2 mpsi and a rise time of 2 μs.

Pressure in the test section is measured by two pressure gauges (MKS Baratron Type 127A). One gauge has a full-scale range of 1000 mmHg and an accuracy of 0.1

mmHg while the other has a full-scale range of 10 mmHg and an accuracy of 0.001 mmHg. Both are protected against overpressure by remotely controlled valves which should be closed prior to testing. Additionally, Nupro Excess Flow valves provide auxiliary protection. Two Sensotec valves measure initial pressure in the driver and intermediate sections.

Omega SG-2/350-LY11 strain gauges are embedded in the concrete cylinder to measure the time instants of the propagating shock wave. The strain gauges have a resistance of 350 ohms and tolerance level of 0.3%. The strain gauges are soldered to lead wires and immersed in shellac (from beeswax) for insulation. A strain gauge is shown in the Fig. 3.4.

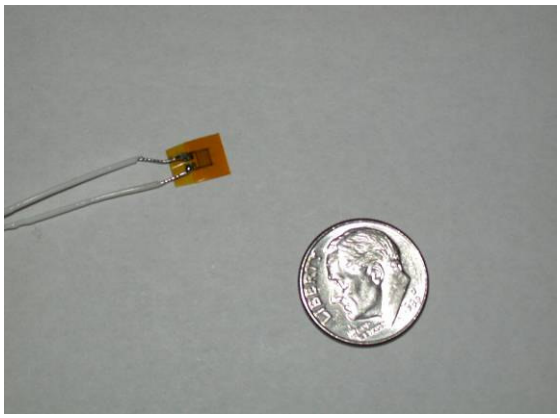

Figure 3.4 A strain gauge (7 mm × 2 mm) compared to a dime.

Each gauge is connected to a Wheatstone bridge circuit as shown in Fig. 3.5. The two ratio arms of the bridge (R1 and R3) are set equal to each other. The variable resistor (R2 in the diagram) is set at a value equal to the strain gauge resistance before the experiment (when no force is applied on the gauges) to balance the setup i.e. the output voltage is zero. A DC power supply provides an excitation voltage of 1.9 volts to the circuit.

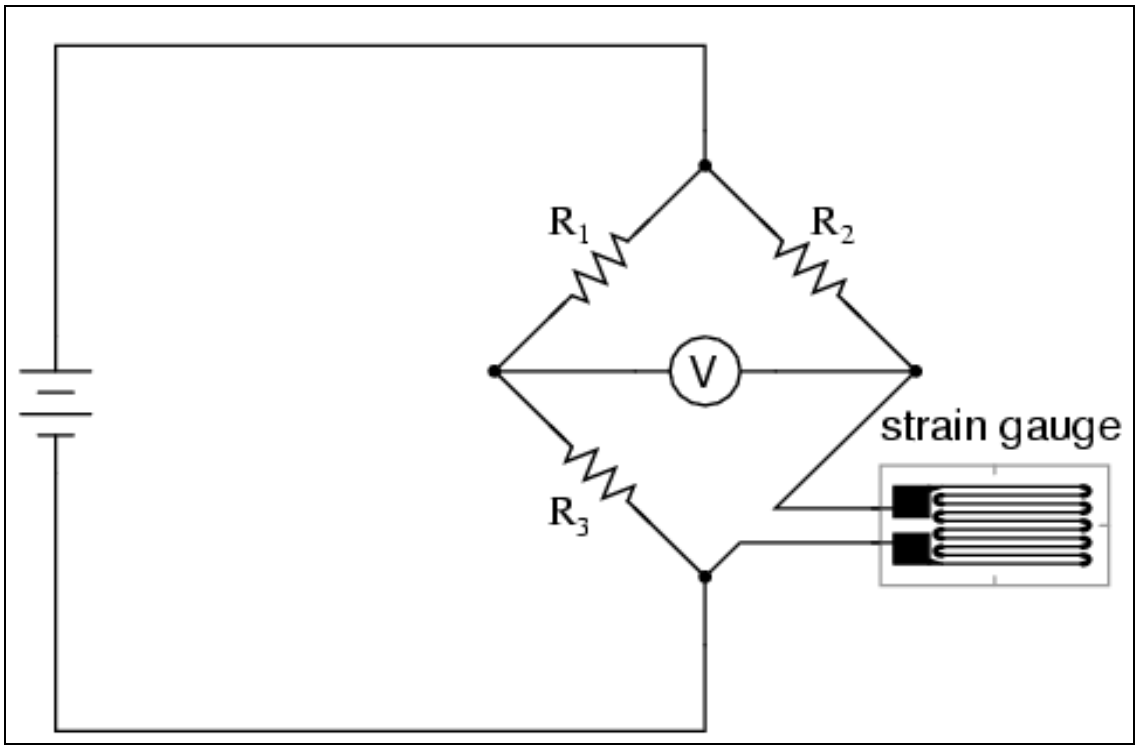

Figure 3.5 Schematic of a Wheatstone Bridge Circuit.

Thus, with no force applied to the strain gauge, the bridge will be symmetrically balanced and the output will indicate zero volts, representing zero force on the strain gauge. As the strain gauge is either compressed or tensed, its resistance will vary, thus unbalancing the bridge and producing an output voltage for the data acquisition system.

3.3 Diaphragm Development

Diaphragm bursting pressure directly influences the total pressure, or load, delivered to a concrete specimen. On the other hand, shock wave strength is directly related to the initial pressure ratio across the diaphragms P4/P1. High loads may cause the formation of fractures in the specimens which may interfere with internal stress waves. The researcher would be unaware of the fractures without extensive additional

inspection following each simulation. Therefore diaphragms with lower bursting pressure are desirable.

Diaphragms previously developed for the shock tube possessed bursting pressures as low as 2.07 MPa (300 psi), necessitating the development of diaphragms with lower bursting pressures. A series of tests was performed to determine the usability and rupture pressures of different diaphragm materials. Through a series of six tests, 0.41 mm (0.016 in.) aluminum shim stock exhibited bursting pressures that are both consistent and desirable, ranging from 1.00 MPa (145 psi) to 1.09 MPa (158 psi), with a 1.04 MPa (151 psi) mean.

These diaphragms proved much easier to fabricate than previous steel diaphragms. A standard paper cutter or tin snips may be used to cut the shim stock into 6 inch squares. A punch tool was fabricated and used to punch ½ inch dowel holes for alignment. The new diaphragms are easily fabricated and reduce wait time between runs.

3.4 Concrete cylinder

The test section accommodates a standard concrete cylinder 30.5 cm (12 in.) long with 15.2 cm (6 in.) diameter. It is mounted coaxial to an incoming shock wave. The cylinder is protected from reflected shock waves from the vacuum tank and other external surfaces by a steel tube 30.5 cm (12 in.) deep with 17.8 cm (7 in.) inner diameter. A ring on one end of the tube provides support against axial movement. Contact between the cylinder and ring surfaces is damped by a 1.3 cm (0.5 in.) thick neoprene pad. The gap around the cylinder circumference is filled with an expanded polyurethane foam. The neoprene and polyurethane materials hold the specimen securely

while damping both stress wave concentration and interaction with boundaries [8]. Only the front (circular) surface of the cylinder is exposed to the shock wave, perpendicular to the wave propagation. Most of the rear cylinder surface is also unbounded in order to lessen stress wave transmission through the rear boundary as well as to allow scabbing of the specimen. The test section and a photo of the cylinder mounted in the test section is shown in Fig. 3.6.

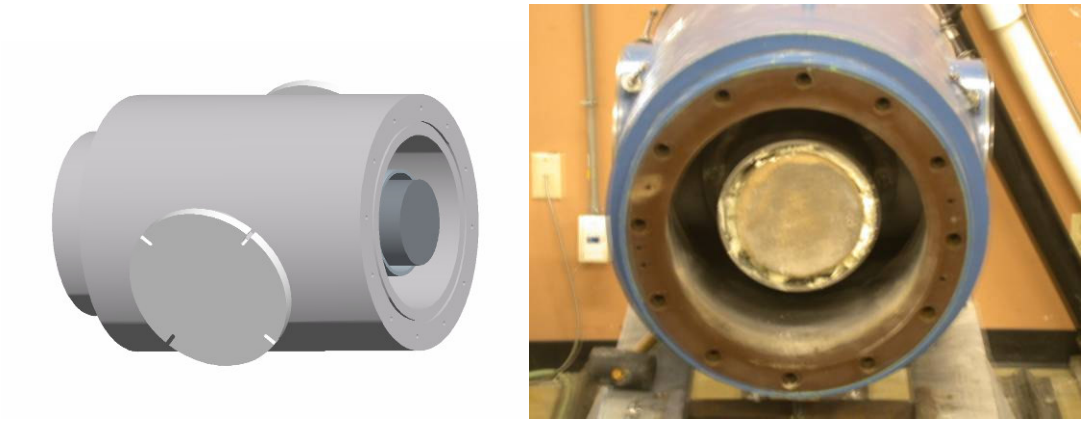

Figure 3.6 Schematic side view and front view on the concrete cylinder mounted in the test section

The composition of the concrete is a very weak mix of cement i.e. high concentration of sand. The mix is based on the composition from investigators at the Institute for High Energy Density, Russian Academy of Sciences, Moscow, Russia. The volume and mass compositions for casting five cylinders are found in Table 3.1.

Table 3.1 Composition of the cement mixture

Components	Volume	Mass
Water	13.5L (3.6 gal)	13.5 kg (29.8 lb)
Cement (TXI Type I/II Portland Cement)	3L (0.8 gal)	3.6 kg (7.9 lb)
Sand(Sakrete All-Purpose Sand manufactured by Texas Industries, Inc. (TXI)).	45L (11.9 gal)	73.3 kg (161.6 lb)

Sieve analysis was conducted on the sand and the fineness modulus was found to be 3.1. The particle size distribution is shown in Fig. 3.6

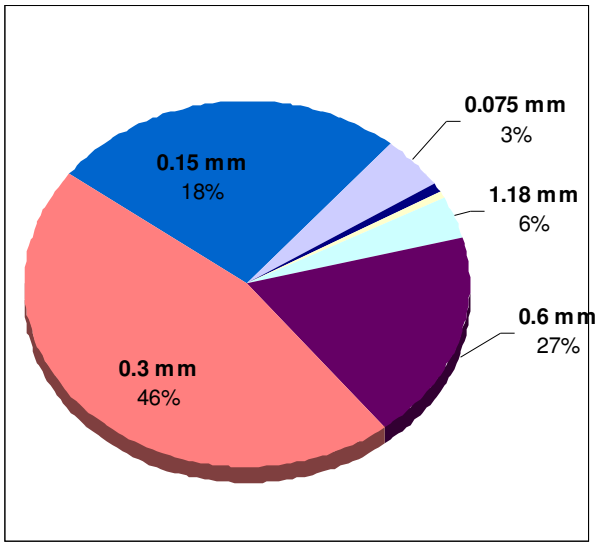

Figure 3.6 Particle Size Distribution of the sand.

Dry sand and cement are mixed together for 5 minutes in the concrete mixer. After the sand and cement have been thoroughly mixed, water is added and mixer is run for another 10 minutes till the mixture is ready. The mixture is subjected to a slump test and a 2.5 cm (1 in.) slump is noted. The cylinders are cast in 304.8 mm (12 in.) plastic molds of diameter 152.4 mm (6 in.). Two strain gauges are embedded in the cylinder

while casting. The strain gauges are placed 101.6 mm (4 in.) apart. The other two strain gauges are mounted on the two ends of the cylinder using epoxy. Immediately after casting, the molds were placed in a curing room and remained there for seven days before the cylinders are removed for testing.

3.5 Error Analysis

The basic formula used for error analysis is

$$\left(\frac{\Delta r}{r}\right)^2 = a^2\left(\frac{\Delta x_1}{x_1}\right)^2 + b^2\left(\frac{\Delta x_2}{x_2}\right)^2 + c^2\left(\frac{\Delta x_3}{x_3}\right)^2 + \ldots\ldots\ldots\ldots \quad \text{(4.2)}$$

where the equation used in the calculation is

$$r = kx_1^a x_2^b x_3^c \ldots\ldots\ldots\ldots \quad \text{(4.3)}$$

where k is a constant and x_1, x_2, x_3 are the variables or measured values.

The error in the Mach number calculation is given by

$$\left(\frac{\Delta M}{M}\right)^2 = \left(\frac{\Delta t}{t}\right)^2 + \left(\frac{\Delta d}{d}\right)^2 \quad \text{(4.4)}$$

Here f= 100 kHz and the order of t is 10^{-3} s. Thus

$$\left(\frac{\Delta t}{t}\right) = 0.01 \quad \text{(4.5)}$$

Similarly Δd= 1/16 ^{in}. and d is 54 inches. Thus

$$\left(\frac{\Delta d}{d}\right) = 1.157\ e^{-3} \quad \text{(4.6)}$$

Combining Equations (4.4), (4.5) and (4.6) we get

$$\left(\frac{\Delta M}{M}\right)=0.011 \qquad \text{.....(4.7)}$$

The Mach number calculations are within a limit of 1.1%.But this is not true in case of wave speed propagation as the placement of the strain gauge in the cylinder can be off up to $1/4^{th}$ of an inch in 4 inches due to human error. Therefore

$$\left(\frac{\Delta d}{d}\right)= .0625 \qquad \text{.....(4.8)}$$

The error in t remains the same as it depends on the Data Acquisition system. Therefore the error in wave speed can be as high as 6.3%.

The error in pressure calculation is given by

$$\left(\frac{\Delta p_{total}}{p_{total}}\right)^2 = \left(\frac{\Delta p_{measured}}{p_{measured}}\right)^2 + 4*\left(\frac{\Delta M}{M}\right)^2$$

$\left(\frac{\Delta p_{measured}}{p_{measured}}\right)$ is the accuracy in the Baratron transducer used to measure the vacuum pressure ahead of the wave and if found to be ±4%. Therefore the error in total pressure calculation is around 4.6%.

CHAPTER 4

RESULTS AND DISCUSSIONS

4.1 Test Matrix

Twelve cylinders were tested over pressure ratios (the ratio between the high pressure in the driver tube and the vacuum in downstream i.e. p4/p1) of approximately 200, 250, 350, 400, 450, 550 and 600, with a number of repeats. Variation of pressure ratios helped us to vary the stagnation pressures of the shock wave i.e. the impact pressures of blast wave on the cylinders. The downstream was evacuated to around 6894.7 Pa (1 psia). The driver pressure was varied depending on the ratio required. Strain gauges placed on end faces of the concrete cylinder and embedded within the cylinder were used to determine the instants of shock propagation in the cylinder. The cylinders were photographed after the test for a qualitative study. A study on the shock speeds through the concrete is presented in section 4.3. Table 4.1 shows the preliminary test result of different samples. As you can see from the table, the actual pressure ratio is always lower than the estimated pressure ratio. Two of the twelve tests were unsuccessful – there was a premature rupture of diaphragm in the first case and downstream leakage leading to increase in vacuum pressure in the other. In few cases, the strain gauges malfunctioned and this led to loss of data. Samples 9 to 12 represent repeats of the previous tests.

Table 4.1 Preliminary Test Result

Sample	Estimated Pressure ratio	Driver Pressure (psia)	Driver Pressure (MPa)	Vacuum pressure (psia)	Vacuum pressure (Pa)	Actual Pressure ratio	Result	Comment
1	200	208	1.43	1.157	7977.2	180	Successful	
2	250	253	1.74	1.116	7694.5	227	Successful	
3	400				0		Unsuccessful	Premature rupture of diaphragm
4	600	602	4.15	1.529	10542	394	Successful	Gauge 4 malfunctioned
5	350	349	2.41	1.157	7977.2	302	Successful	
6	450	449	3.1	1.34	9238.9	335	Successful	Gauge 3 malfunctioned
7	550	560	3.86	2.214	15264.9	253	Unsuccessful	Vacuum leak leading to large variation in pressure ratio Gauge 4 malfunctioned
8	400	402	2.77	1.026	7074	392	Successful	
9	200	206	1.42	1.059	7301.5	195	Successful	Gauges 2 & 4 malfunctioned
10	250	254	1.75	1.167	8046.1	218	Successful	Gauge 4 malfunctioned
11	600	596	4.11	1.145	7894.4	521	Successful	Gauge 3 malfunctioned
12	400	404	2.79	1.033	7122.2	391	Successful	Gauges 2 & 4 malfunctioned

4.2 Test Results

4.2.1 Sample 1

The estimated pressure ratio for sample 1 was 200. The driver tube was charged to 1.43 MPa (208 psia) and the downstream vacuum was 7908.2 Pa (1.147 psia) which resulted in a pressure ratio of 180. The pressure plots are shown in Figure 4.1. The two pressure transducers kept at a distance of 54 inches apart as shown in Table 4.1. The strains are shown in Figure 4.2. The first two gauges are presented on left hand and the other two are on the right hand side scale. This shows attenuation of wave strength by the time the wave reaches the last two gauges.

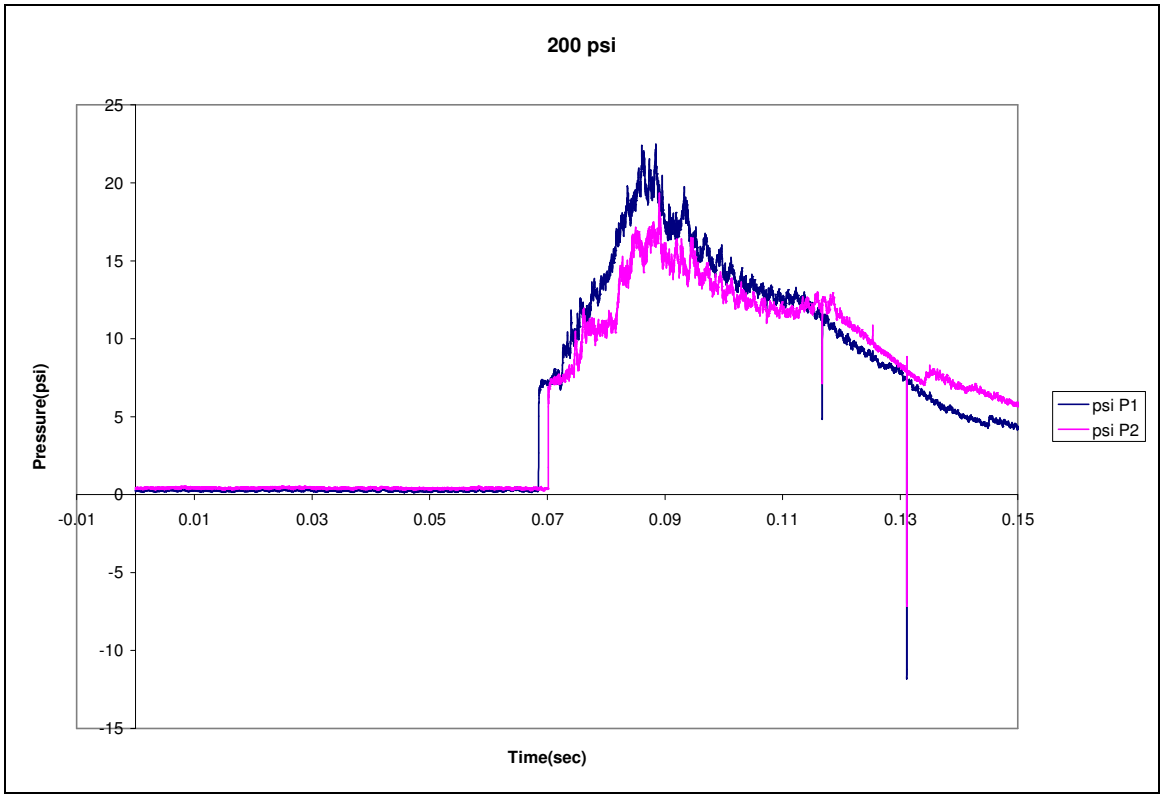

Figure 4.1 Pressure histories for the propagating shock wave of Sample 1.

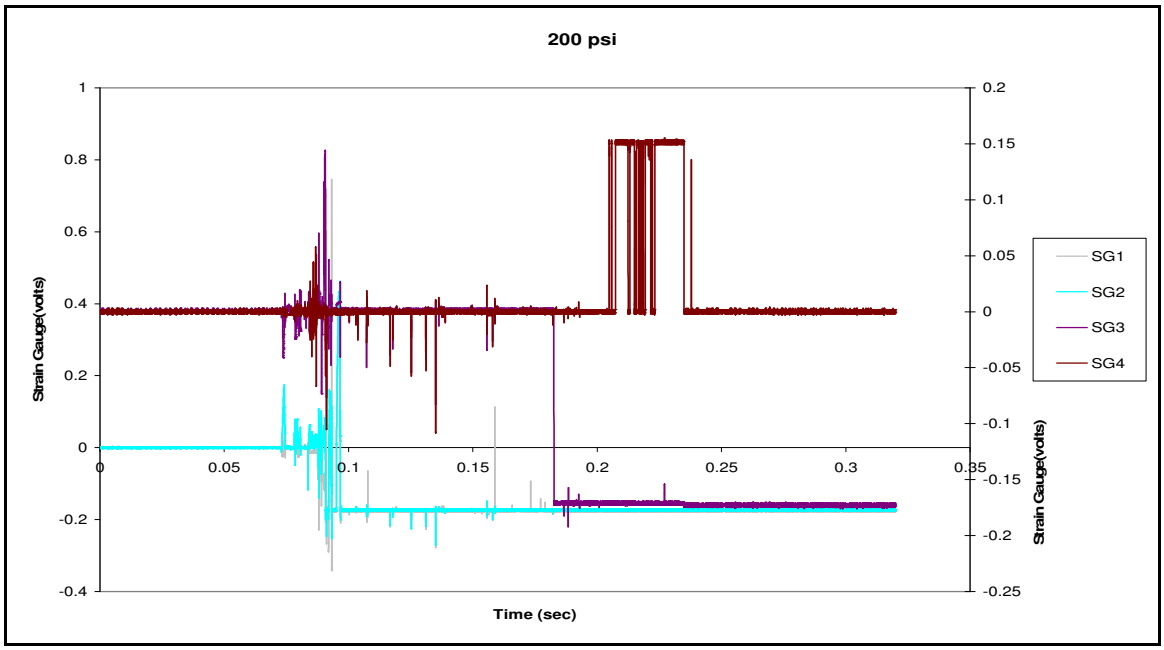

Figure 4.2 Strain gauge outputs of Sample 1.

In the above graph the voltage suddenly drops to negative values which remain almost constant from then in the gauges 1, 2 and 3. This can be attributed to the breaking of the wires connected to the gauges. Gauge malfunctioning results in the plateau formation in the plot of gauge 4.

The photographs of the cylinder before and after the test are shown Figure 4.3.

(a)

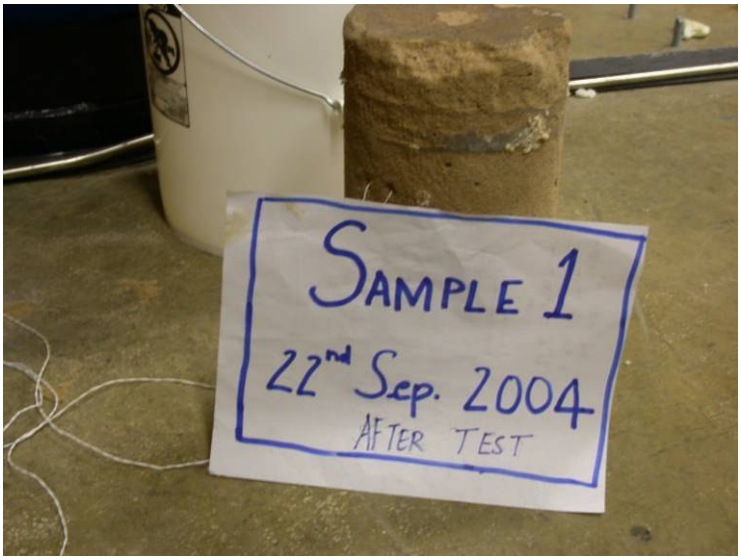

(b)

Figure 4.3 Sample 1 (a) before test and (b) after test with the distal face shown.

As it can been seen from the strain gauge plots there is attenuation in the shock wave strength as the wave passes through the concrete cylinder. Also from the photograph of the sample, it is observed that there is chipping of on the distal face of the cylinder. This shows that there is a strong effect of wave reflection which leads to tension

in the concrete. Such spallation has been observed in materials damage by shock and blast [2].

4.2.2 Sample 2

The estimated pressure ratio for sample 2 was 250. The driver tube was charged to 1.74 MPa (253 psia) and the downstream vacuum pressure was 7964.5 Pa (1.116 psia) which yields a pressure ratio of 227. The pressure plots are shown in Figure 4.4. The Mach number was calculated to be 2.46 as shown in Table 4.2. The strain gauge plots are shown in Figure 4.5, with axes similar to Fig. 4.3. The first two gauges are presented on left hand side and the other two are on the right hand side scale.

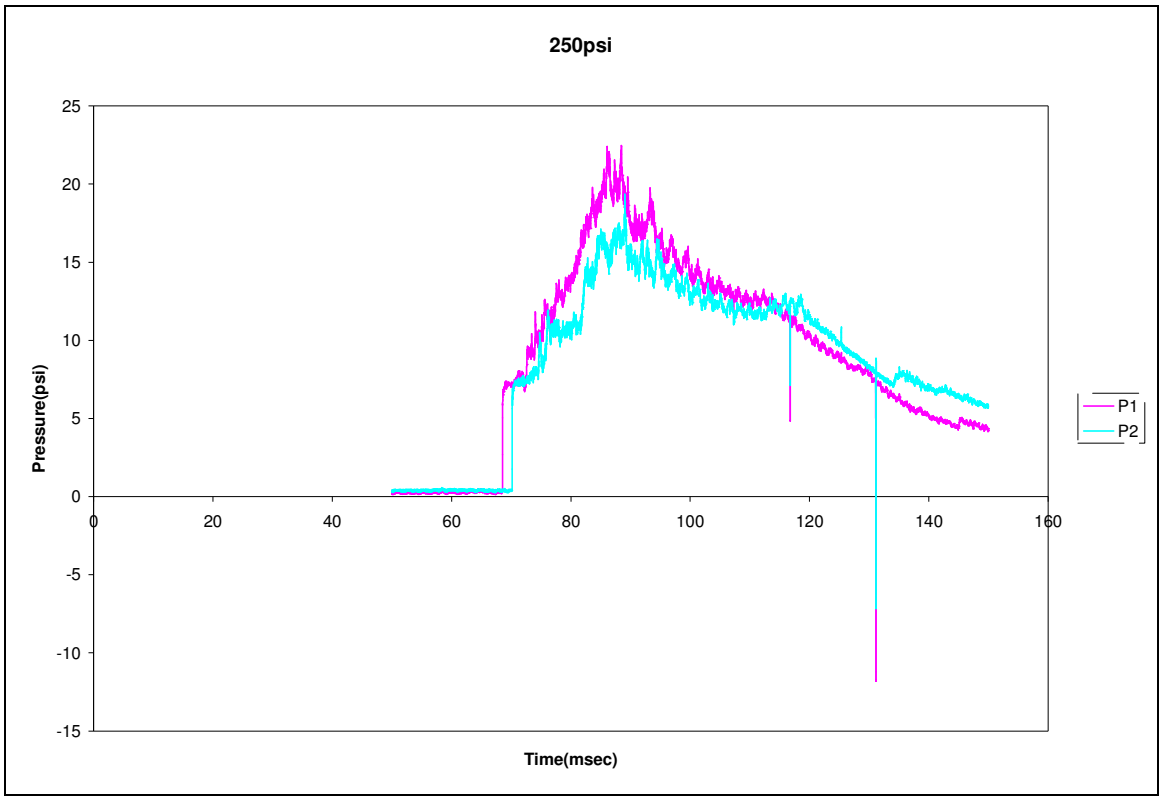

Figure 4.4 Pressure histories for the propagating shock wave of Sample 2.

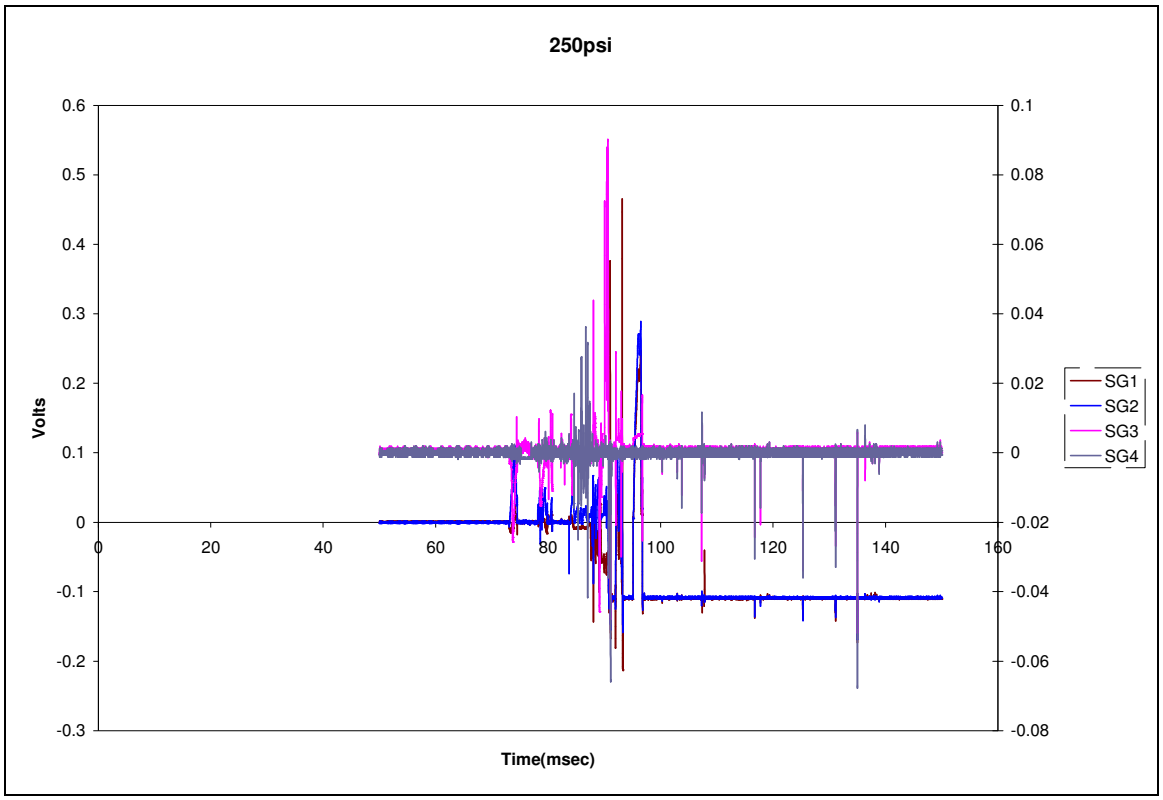

Figure 4.5 Strain gauge outputs of Sample 2.

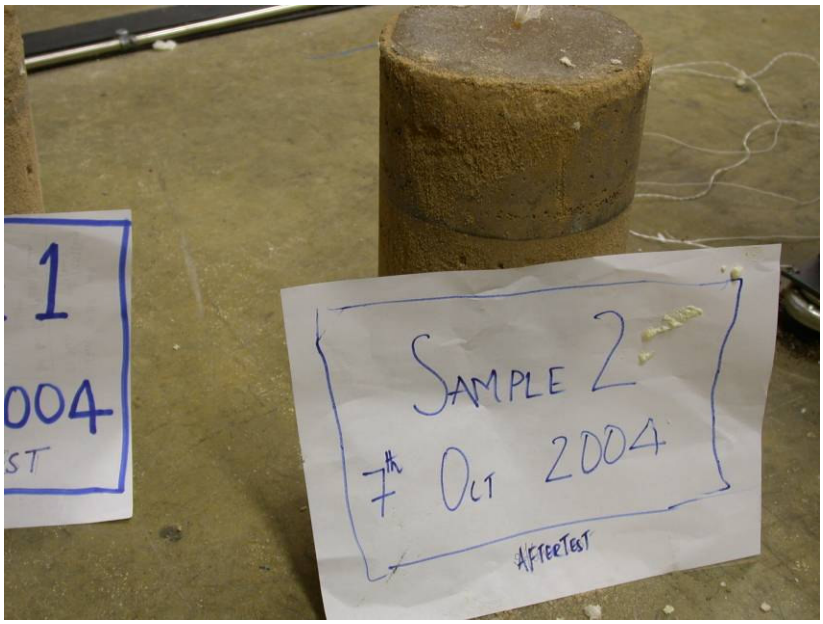

Figure 4.6 Sample 2 with the proximal side up after testing.

As can be seen from Fig. 4.5, the shock strength is attenuated as the wave passes through the concrete cylinder. The wave speeds at different points are via a time-of-flight method and shown in Table 4.2. Visually, there is very little destruction of the proximal face of the cylinder as shown in Figure 4.6. This shows that this concrete mix can withstand the lower strength shocks.

4.2.3 Sample 3

The estimated pressure ratio for this test was 400. Unfortunately, a premature rupture of the secondary diaphragm led to destruction of the strain gauges of the sample before the actual test. As a result there was no data and the test had to be discarded.

4.2.4 Sample 4

The test pressure ratios are shown in Table 4.1. The pressure plots are shown in Figure 4.7. The Mach number was calculated to be 2.69 as shown in Table 4.2. The strain gauge plots are shown in Figure 4.8.

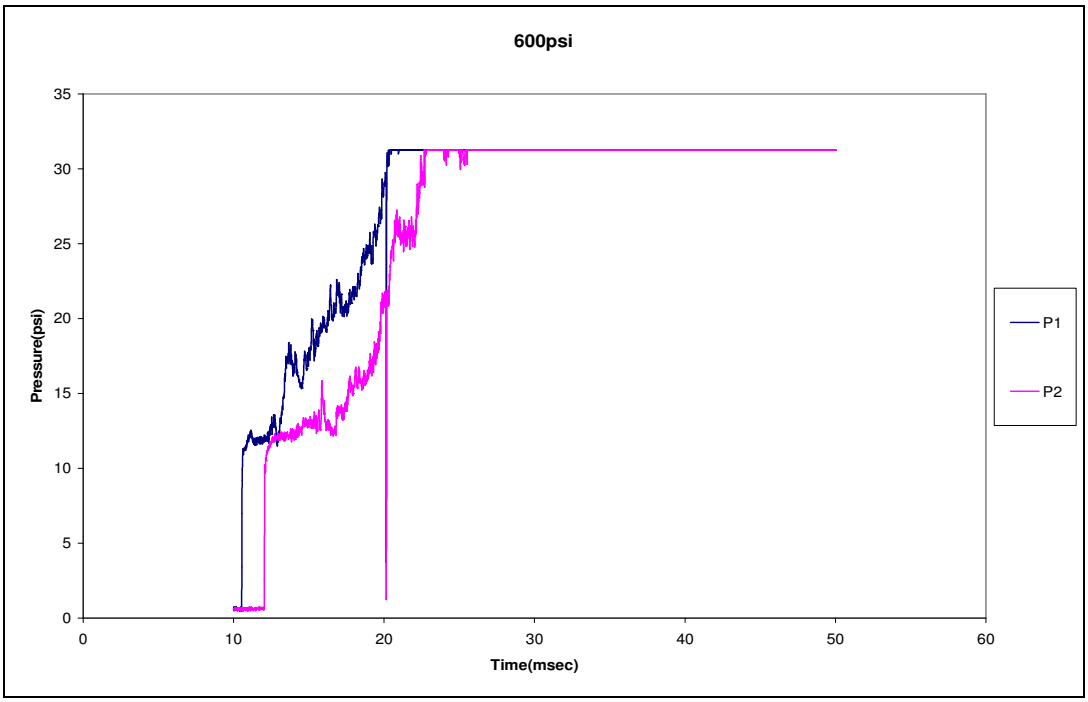

Figure 4.7 Pressure histories for the propagating shock wave of Sample 4.

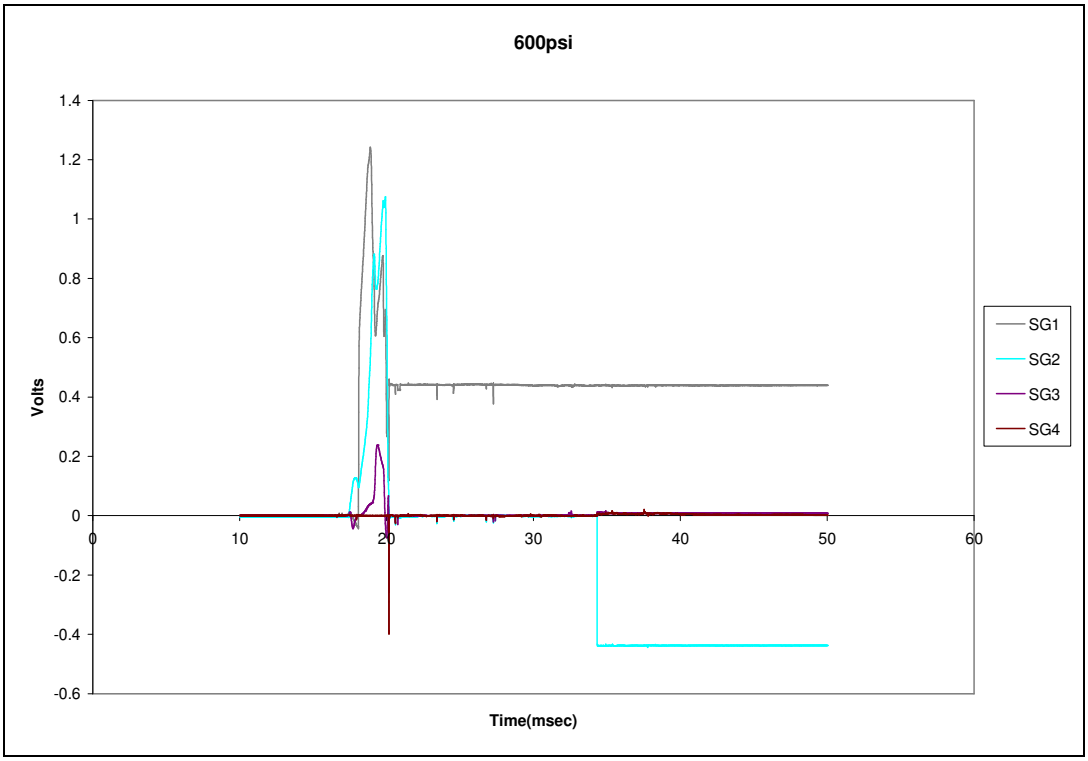

Figure 4.8 Strain gauge outputs of Sample 4.

The photograph of the cylinder in the test section after the blast is shown below.

Figure 4.9 Sample 4 in the test section after the test.

As it can been seen from the above photograph, at high pressures, the cylinder was pushed forward out of the test section. The cracking of the cylinder cannot be fully attributed to the shock wave as can been seen from later tests. The cracking can be due to loose packing material causing the cylinder to crash into its mounts and cracking up. Nonetheless, the shock wave causes more damage on the distal side of the cylinder compared to the proximal side

4.2.5 Sample 5

The test parameters are shown in Table 4.1. The Mach number was calculated to be 2.61 as shown in Table 4.2. The strain gauge plots are shown in Figure 4.11.

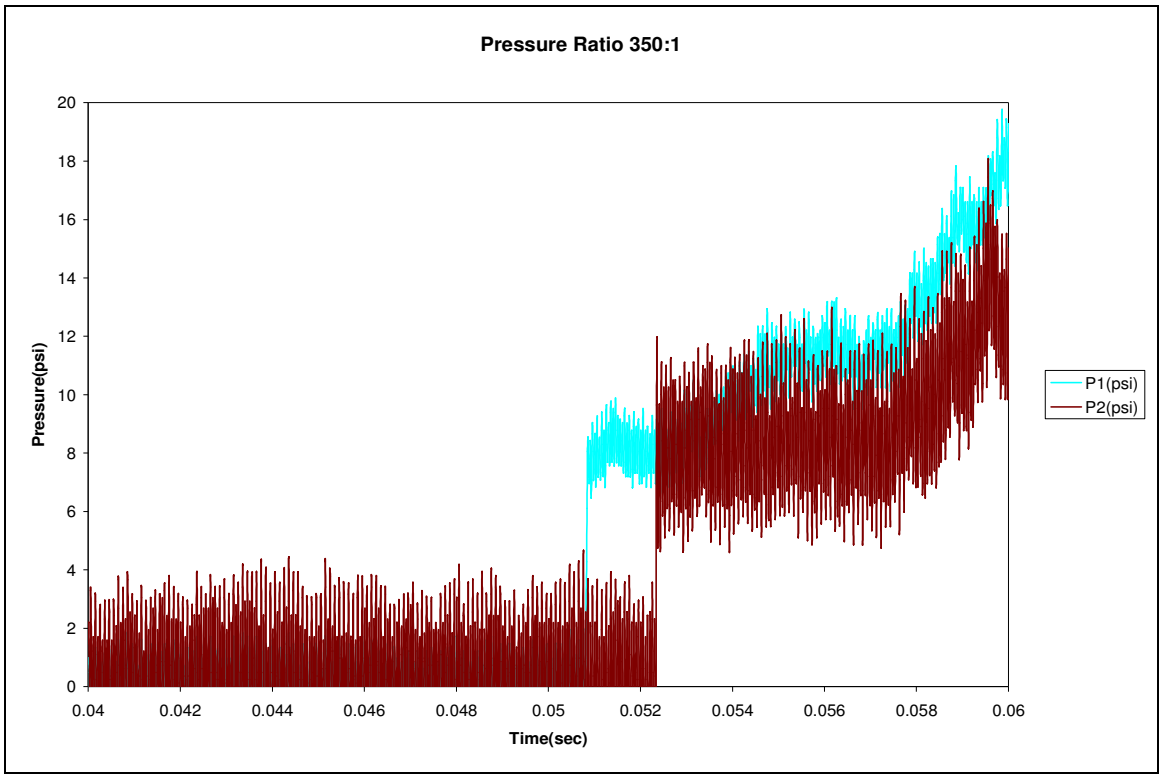

Figure 4.10 Pressure histories for the propagating shock wave of Sample 5.

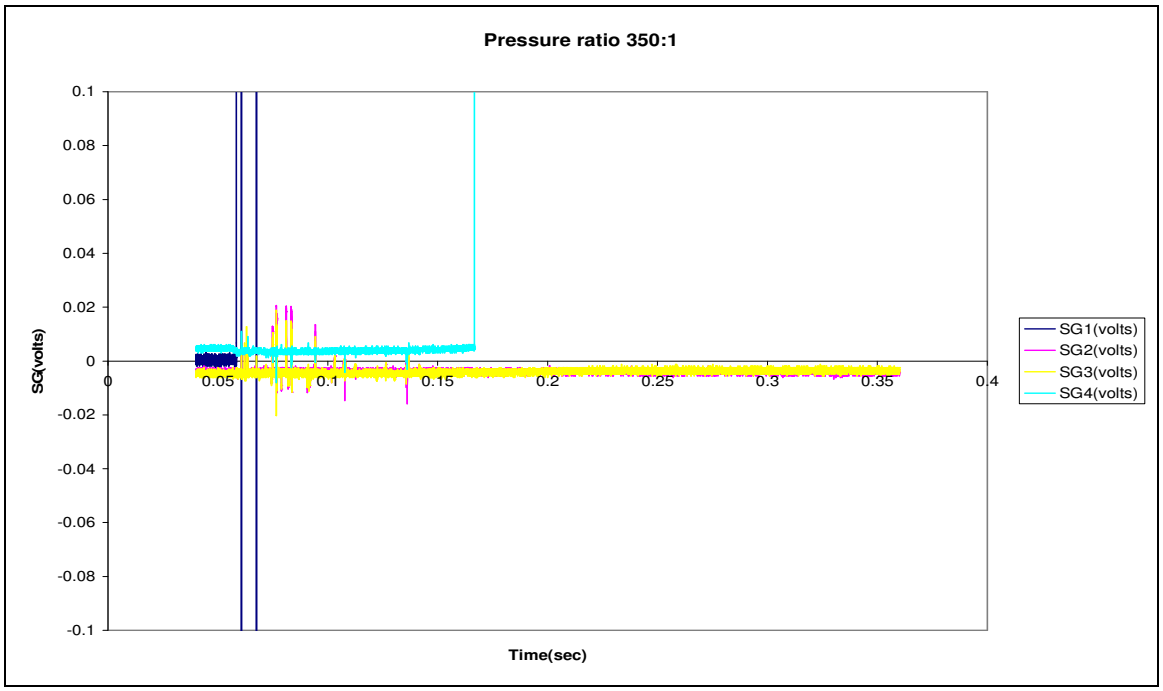

Figure 4.11 Strain gauge outputs of Sample 5.

The data has two spikes beyond ranges for strain gauges 1 and 4 as they broke off after shock wave has passed through. As can been seen from the graph, the shock is attenuated. The photograph below shows that the cylinder was pushed forward from the test section due to the effect of the reflecting shock wave. There was more damage on the distal than the proximal side. As can been seen from the photograph the proximal side also has a bit of damage at these ratios compared to the lower ratios before.

Figure 4.12 Sample 5 in the test section after the test.

4.2.6 Sample 6

The Mach number was calculated to be 2.71 as shown in Table 4.2 based on ratios in Table 4.1. The pressure and strain gauge plots are shown in Figures 4.13 and 4.14.

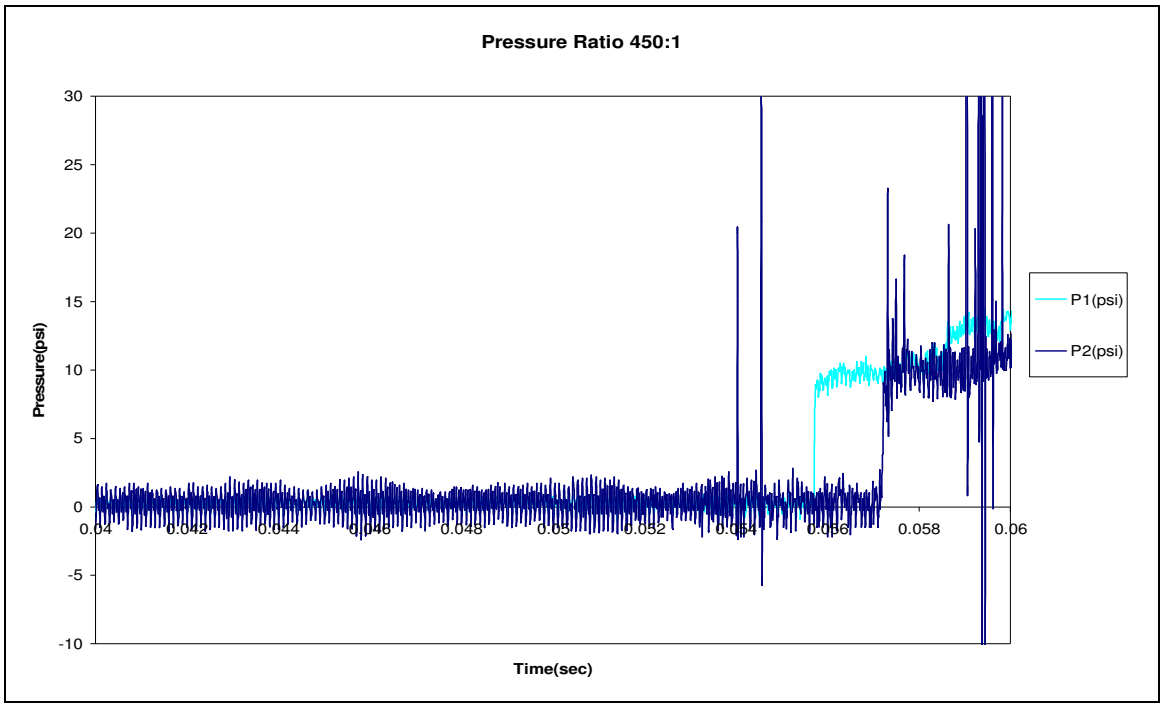

Figure 4.13 Pressure histories for the propagating shock wave of Sample 6.

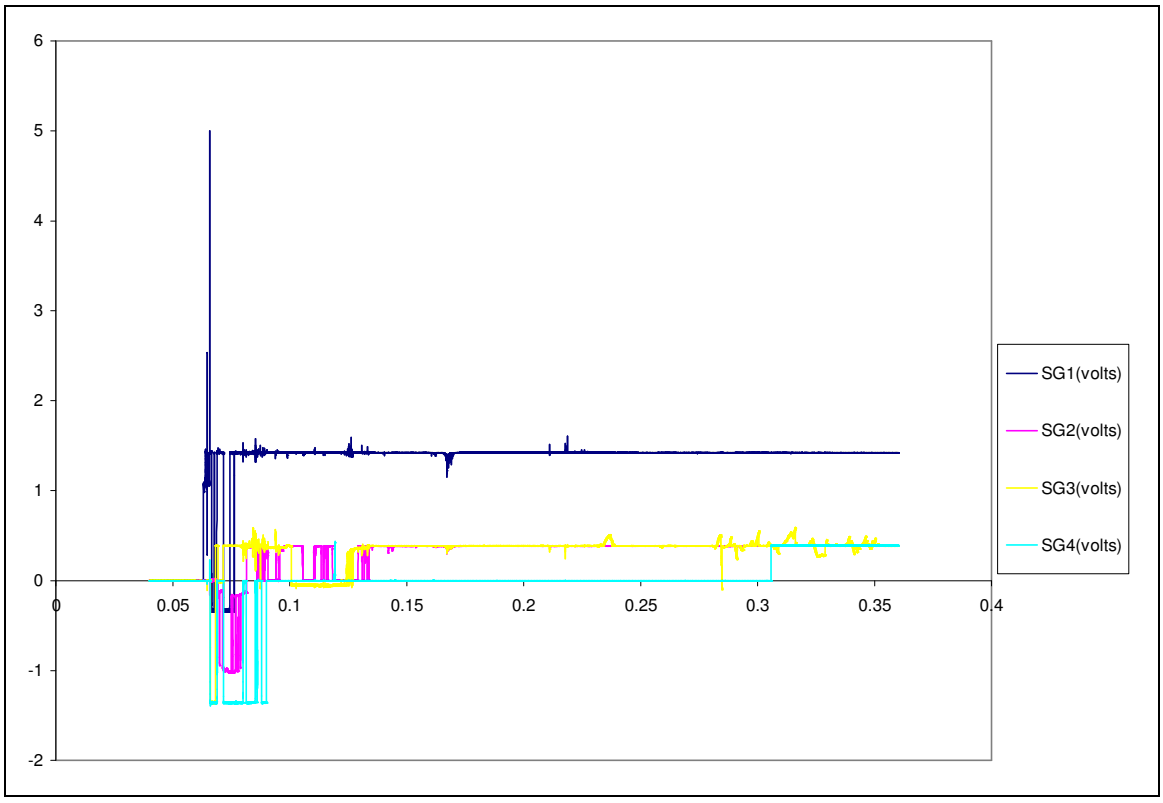

Figure 4.14 Strain gauge outputs of Sample 6.

Figure 4.15 Test Section and the cylinder in the nozzle section after the test of Sample 6.

The data of this test appears noisy. This can be attributed to the vibration due to movement of the concrete cylinder within the test section after the shock wave impact. Finally the shock reflection off the distal face pushed the cylinder forward resulting in the breakage of the strain gauges. The maximum damage occurred on the proximal side of the cylinder.

4.2.7 Sample 7

The estimated pressure ratio for sample 7 was 550. There was a leak in the vacuum downstream as a result of which we could not maintain the ratio we required. The driver tube was charged to 3.86 MPa (560 psia) and the downstream vacuum pressure was 15264.9 Pa (2.214 psia) which is a pressure ratio of 253. The pressure plots are shown in Figure 4.16. The Mach number was calculated to be 2.71 as shown in Table 4.2. The strain gauge plots are shown in Figure 4.17. Gauge 1 and 4 are on the left hand scale and the other two gauges are represented on the right hand scale. This is due to the fact that 1 and 4 broke off outputting signals beyond the range.

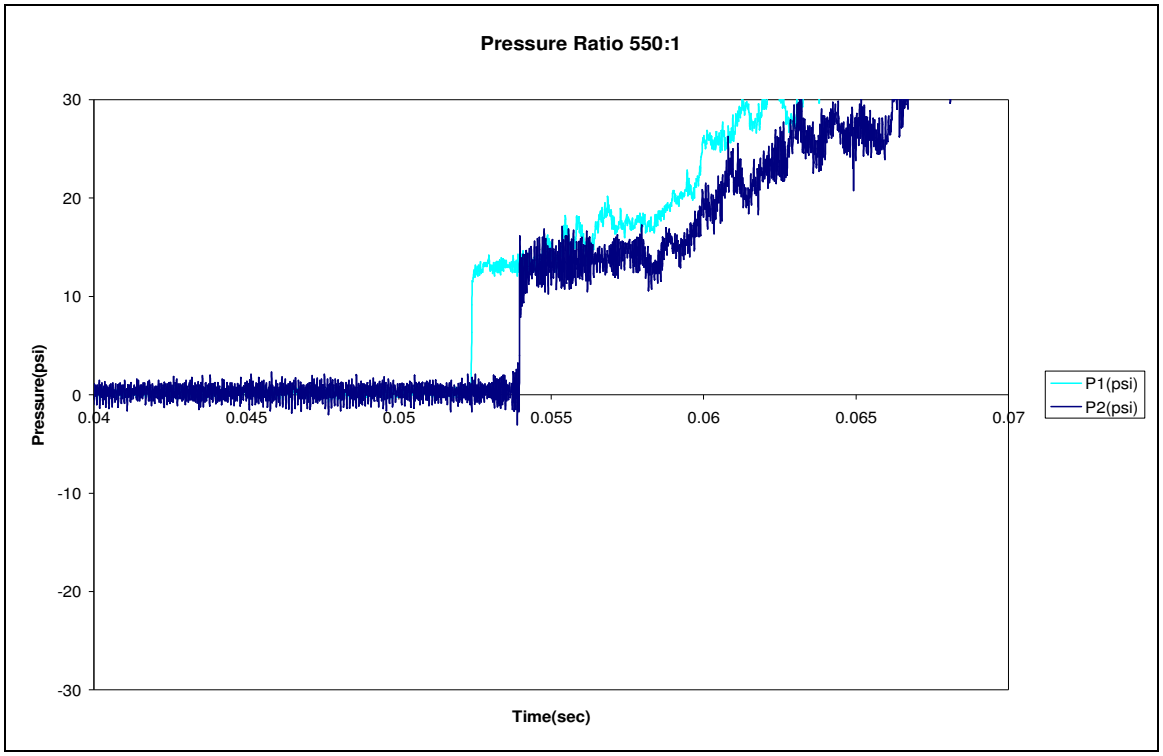

Figure 4.16 Pressure histories for the propagating shock wave of Sample 7.

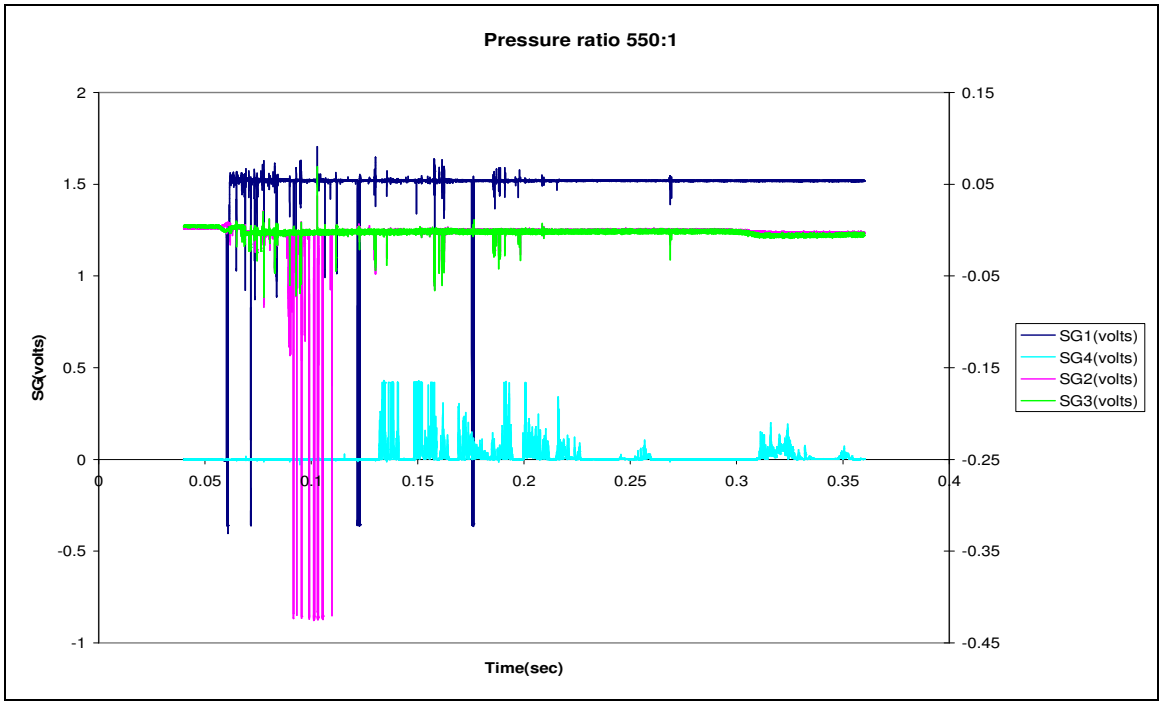

Figure 4.17 Strain gauge outputs of Sample 7.

The photograph of the test is shown below

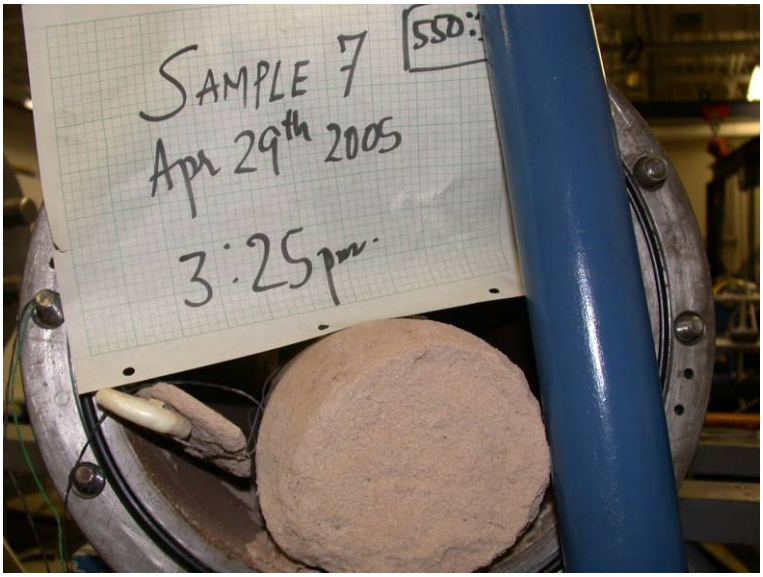

Figure 4.18 Sample 7 in the test section after the test.

The proximal side of the cylinder suffered damage. As one can see from the strain gauge plots, the shock wave was heavily attenuated. The first and last gauge broke off as a result of which there is a lot of noise in the readings.

4.2.8 Sample 8

The test parameters (Table 4.1) resulted in Mach number of 2.73 as shown in Table 4.2. The pressure and strain gauge plots are shown in Figures 4.19 and 4.20. Gauge 1 and 2 are on the left hand scale and the other two gauges are represented on the right hand scale.

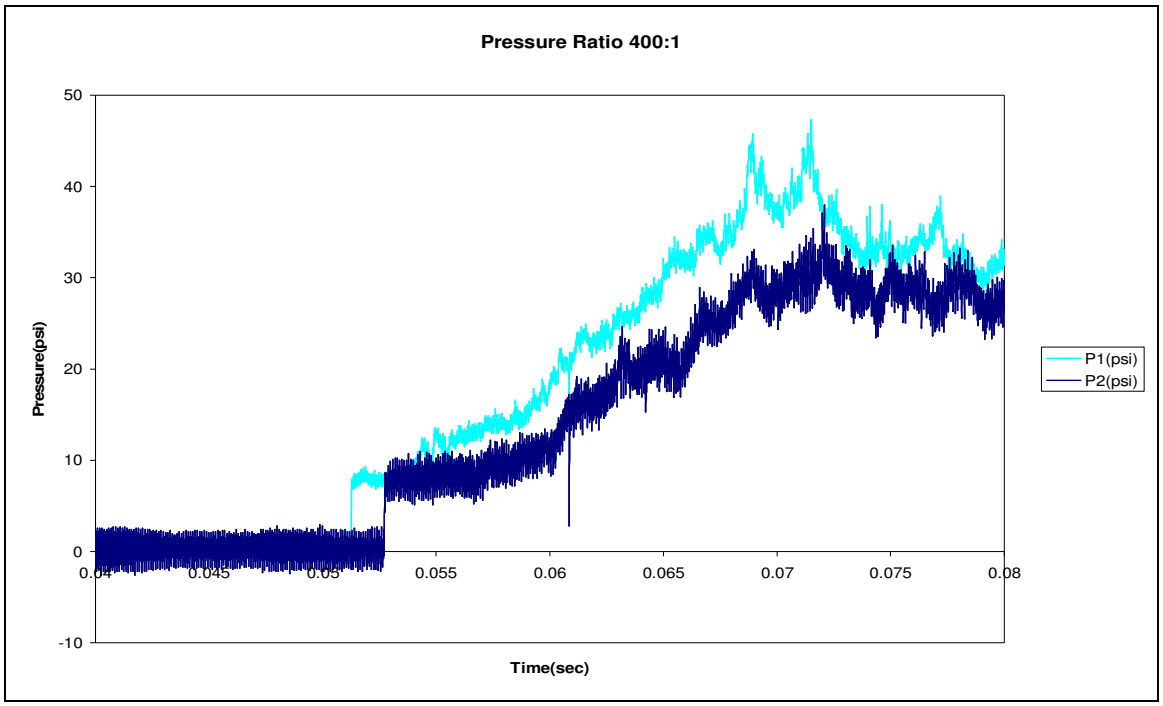

Figure 4.19 Pressure histories for the propagating shock wave of Sample 8.

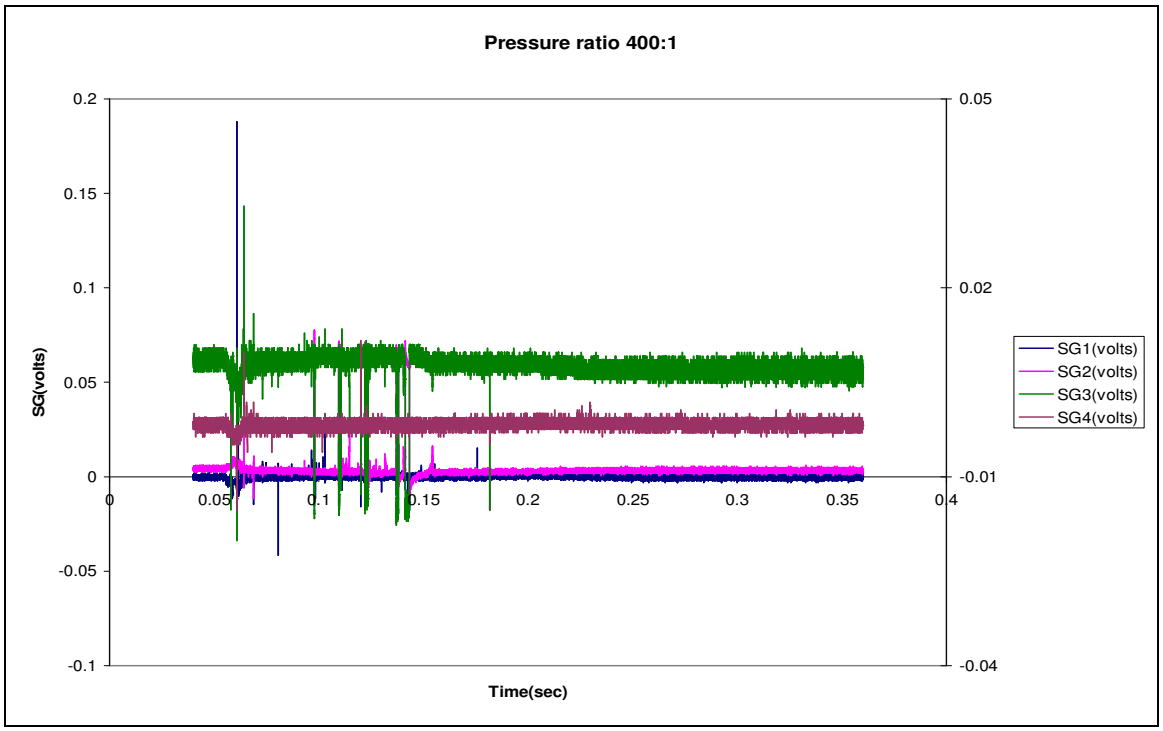

Figure 4.20 Strain gauge outputs of Sample 8.

The photograph of the test is shown below

Figure 4.21 Sample 8 in the test section after the test.

As usual the distal face was damaged more than the proximal side. Therefore the reflecting shock wave was stronger than the incident shock wave. There was attenuation of wave strength as expected.

Samples 9 to 12 are repeats to the above experiments. It was not possible to reproduce the test conditions exactly.

4.2.9 Sample 9

This was a repeat for pressure ratio of 200. The driver tube was charged to 206 psia and the downstream vacuum pressure was 1.059 psia which is a pressure ratio of 194 which was higher than Sample 1. The Mach number was calculated to be 2.47 as shown in Table 4.2. The strain gauge plots are shown in Figure 4.23 where gauge 3 is on the left

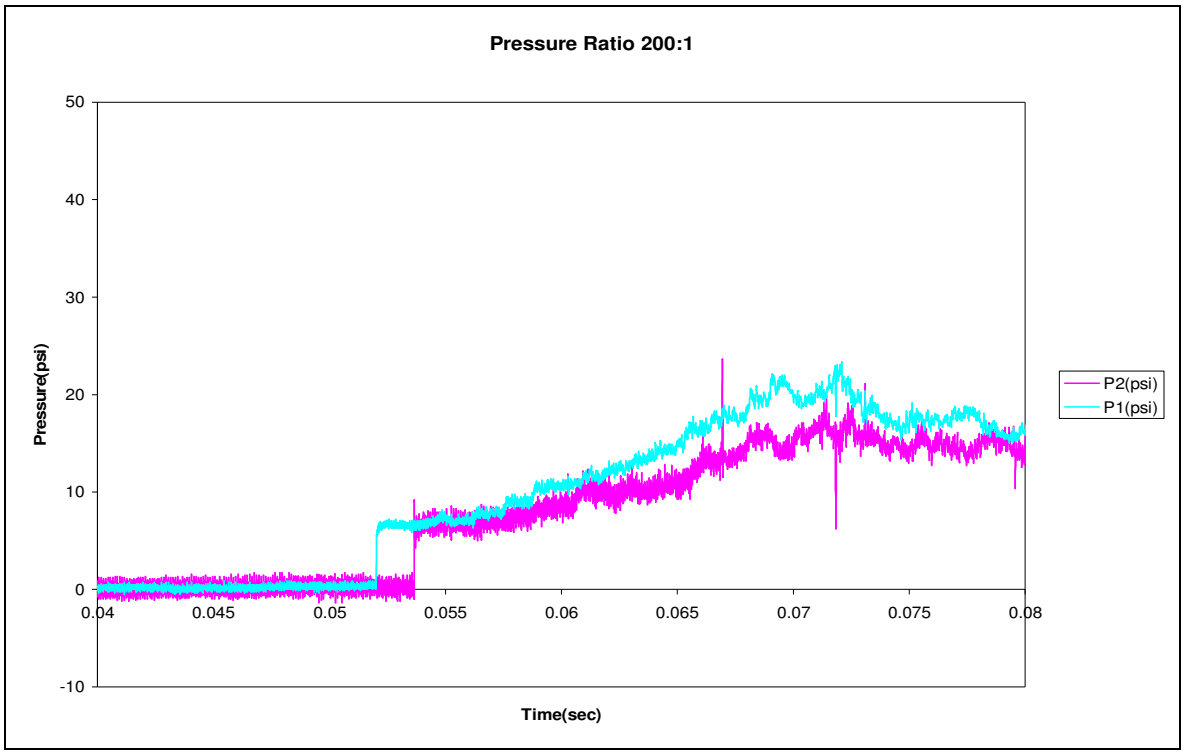

Figure 4.22 Pressure histories for the propagating shock wave of Sample 9.

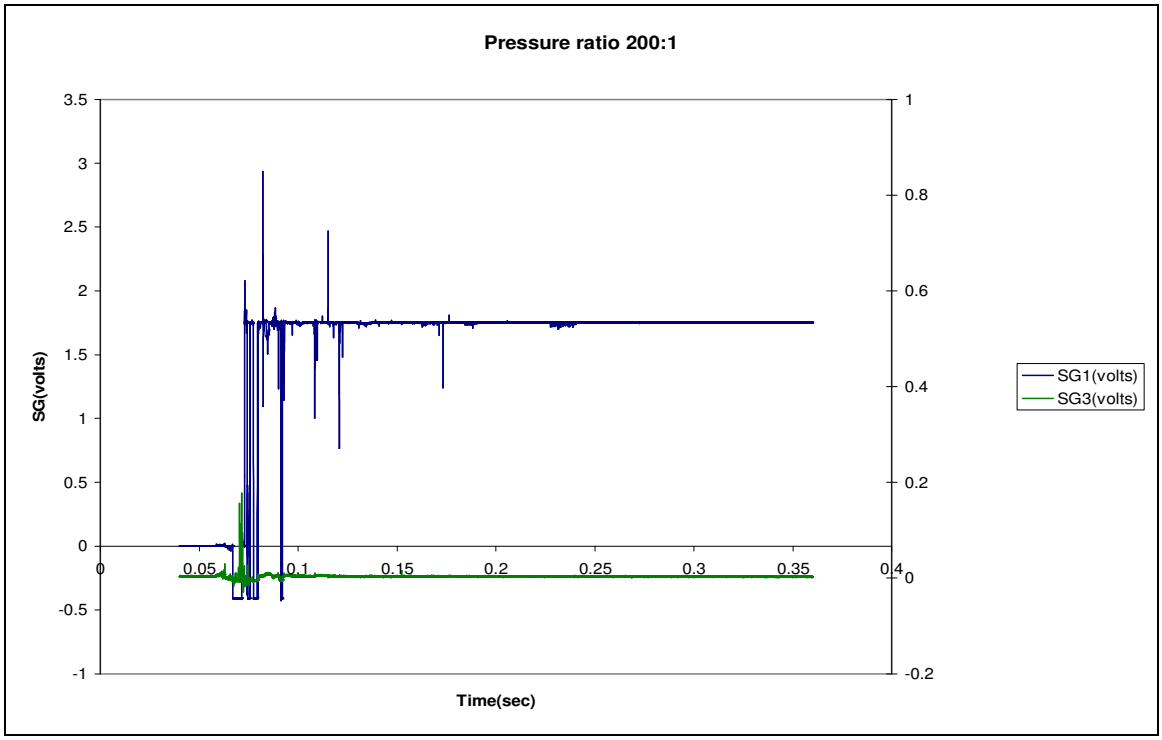

Figure 4.23 Strain gauge outputs of Sample 9.

scale and the other gauges are represented on the right hand scale. Gauges 2 and 4 malfunctioned. The photograph of the test is shown below

Figure 4.24 Sample 9 in the test section after the test.

The cylinder used in test had been used as a test sample earlier. The proximal damage has been occurred due to repeated impacts. As it can be seen from the above figure, the cylinder is still intact in the test section even after the impact. This proves the fact that the cylinder can absorb lower waves of low Mach number.

4.2.10 Sample 10

The parameters are shown in Table 4.1 and the Mach number was calculated to be 2.52 as shown in Table 4.1. The strain gauge plots are shown in Figure 4.26 Gauge 1 is on the left hand scale and the other gauges are represented on the right hand scale. Gauge 4 has malfunctioned and gauge 1 broke off on the impact of the wave.

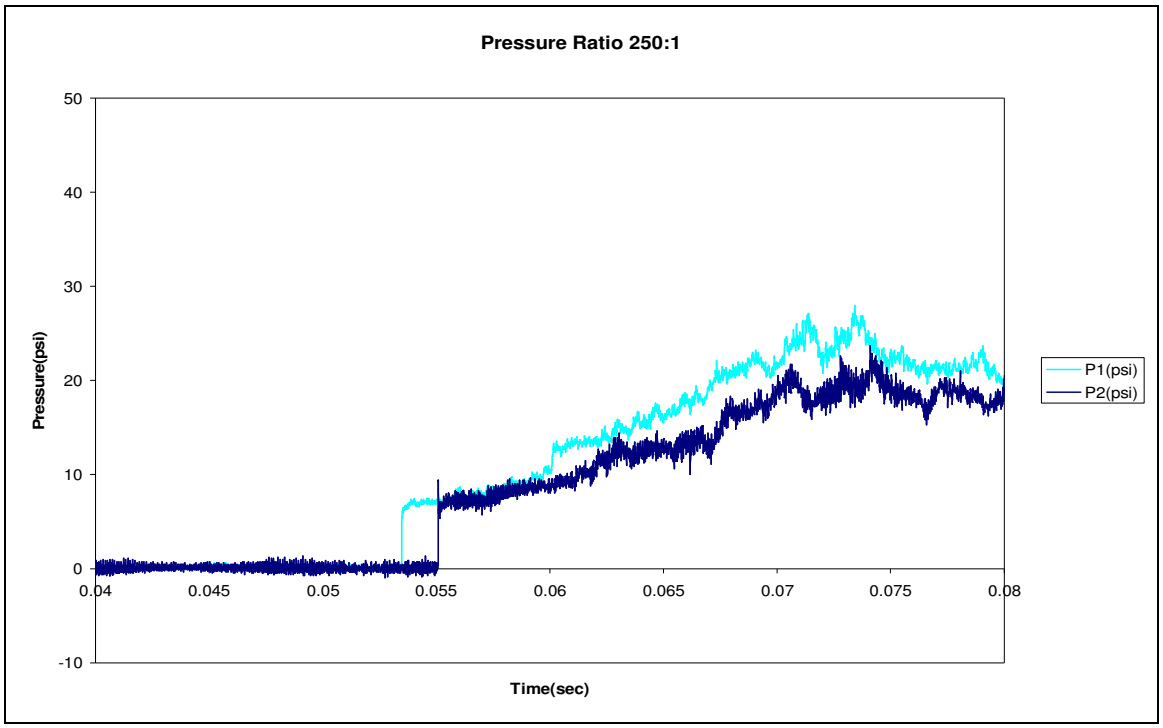

Figure 4.25 Pressure histories for the propagating shock wave of Sample 10.

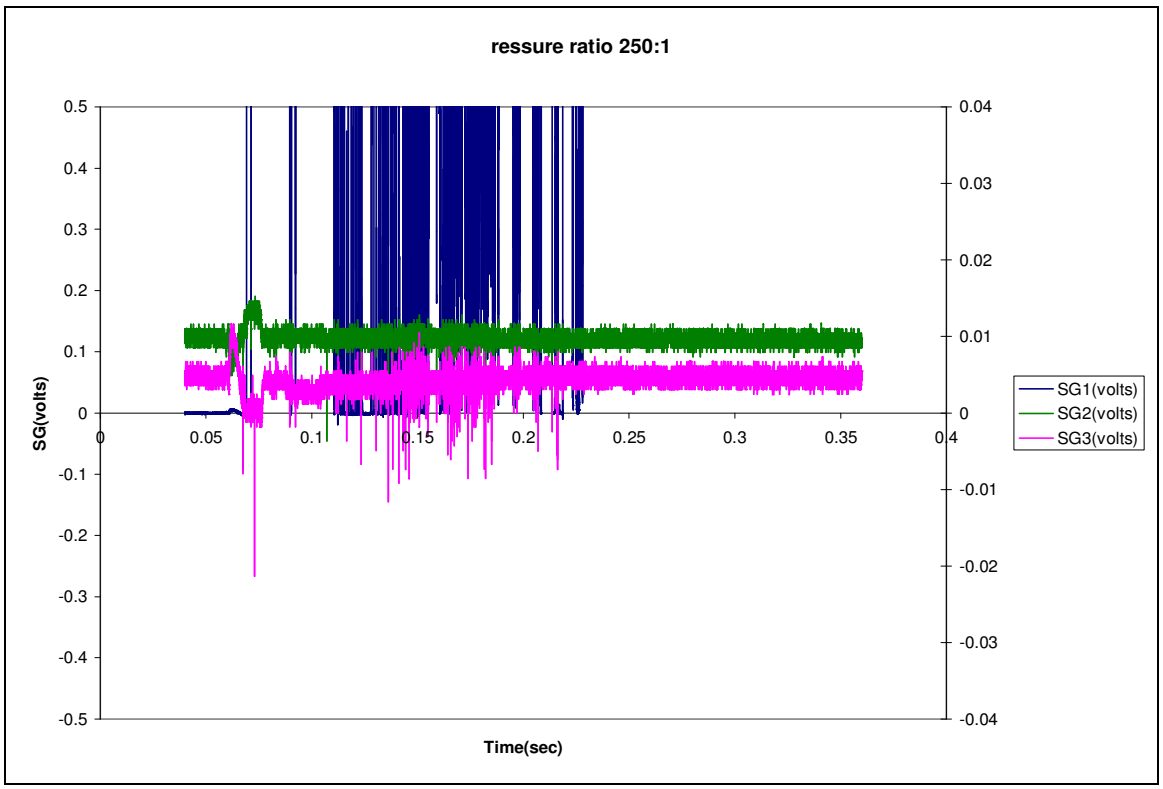

Figure 4.26 Strain gauge outputs of Sample 10.

The photograph of the test is shown below

Figure 4.27 Sample 10 in the test section after the test.

As it can be seen from the above figure, the cylinder hasn't moved out of the test section nor has it cracked up. The range of attenuation is similar to the one in Sample 2.

4.2.11 Sample 11

The Mach number was calculated to be 2.82 as shown in Table 4.1. The strain gauge plots are shown in Figure 4.29 Gauge 1 is on the left hand scale and the other gauges are represented on the right hand scale. Gauge 3 has malfunctioned and gauge 1 broke off on the impact of the wave.

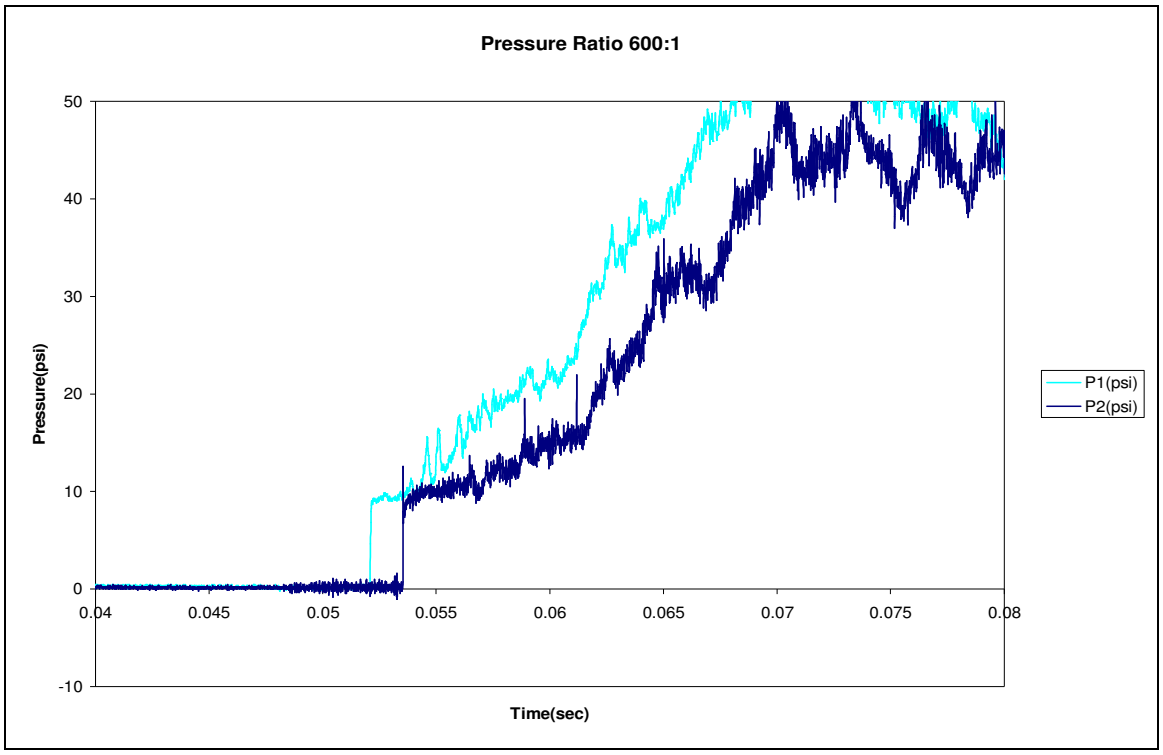

Figure 4.28 Pressure histories for the propagating shock wave of Sample 11.

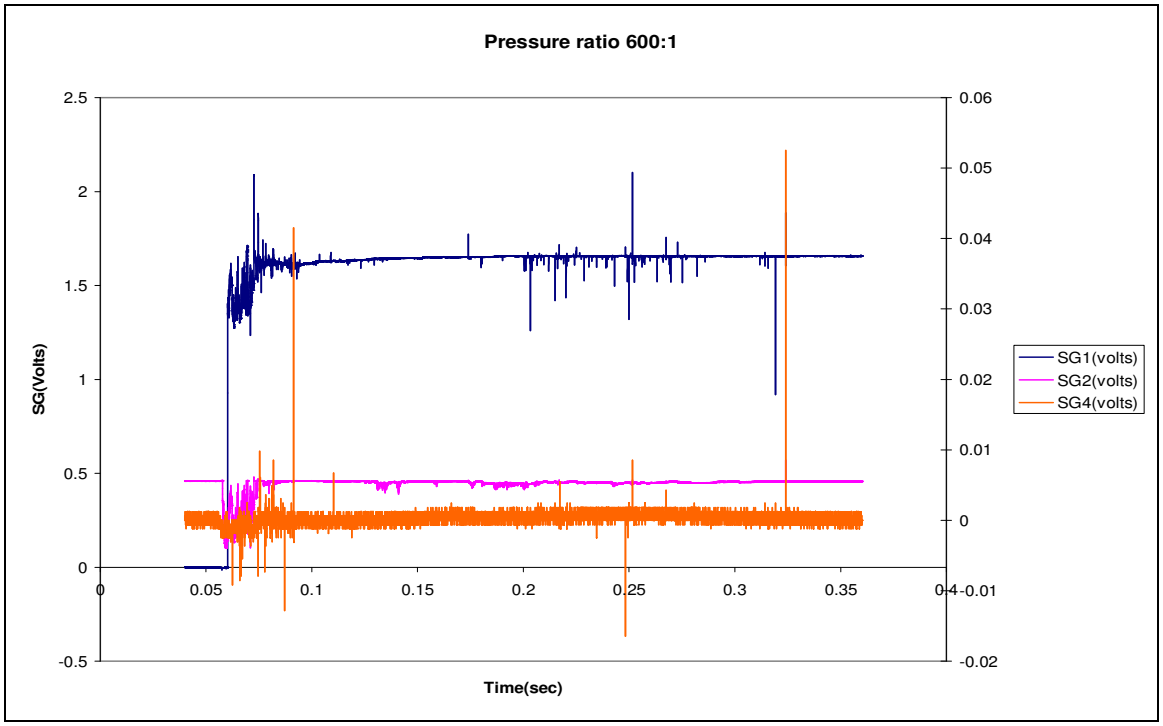

Figure 4.29 Strain gauge outputs of Sample 11.

Figure 4.30 Test Section and the cylinder in the nozzle section after the test of Sample 11

As it can been seen from the above photograph, at high pressures, the cylinder has been pushed forward out of the test section. There is not much data regarding the wave propagation as the gauges broke off. It proves fact that the reflecting shock wave is stronger at higher wave strengths.

4.2.12 Sample 12

This was the best repeat we got as this exactly same as Sample 8. The pressure plots are shown in Figure 4.31. The Mach number was calculated to be 2.82 as shown in Table 4.1. The strain gauge plots are shown in Figure 4.32 Gauge 1 is on the left hand scale and the other gauges are represented on the right hand scale. Gauges 2 and 4 have malfunctioned and gauge 1 broke off on the impact of the wave.

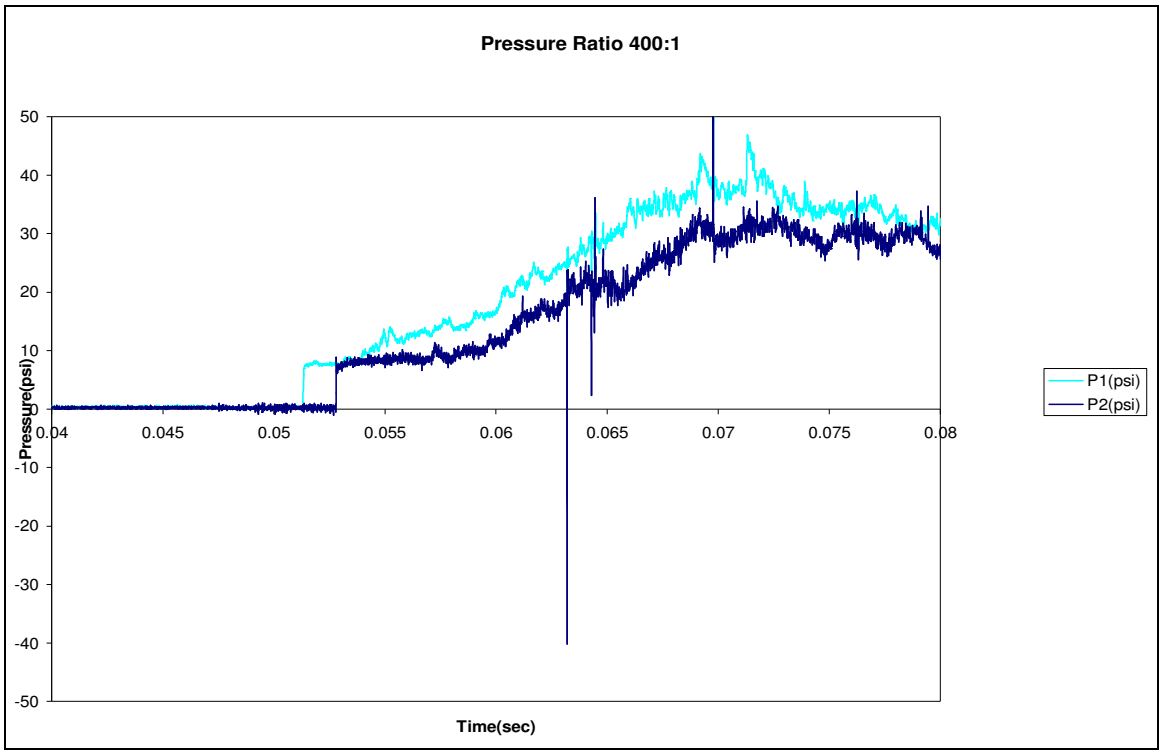

Figure 4.31 Pressure - time plots for the shock wave of Sample 12.

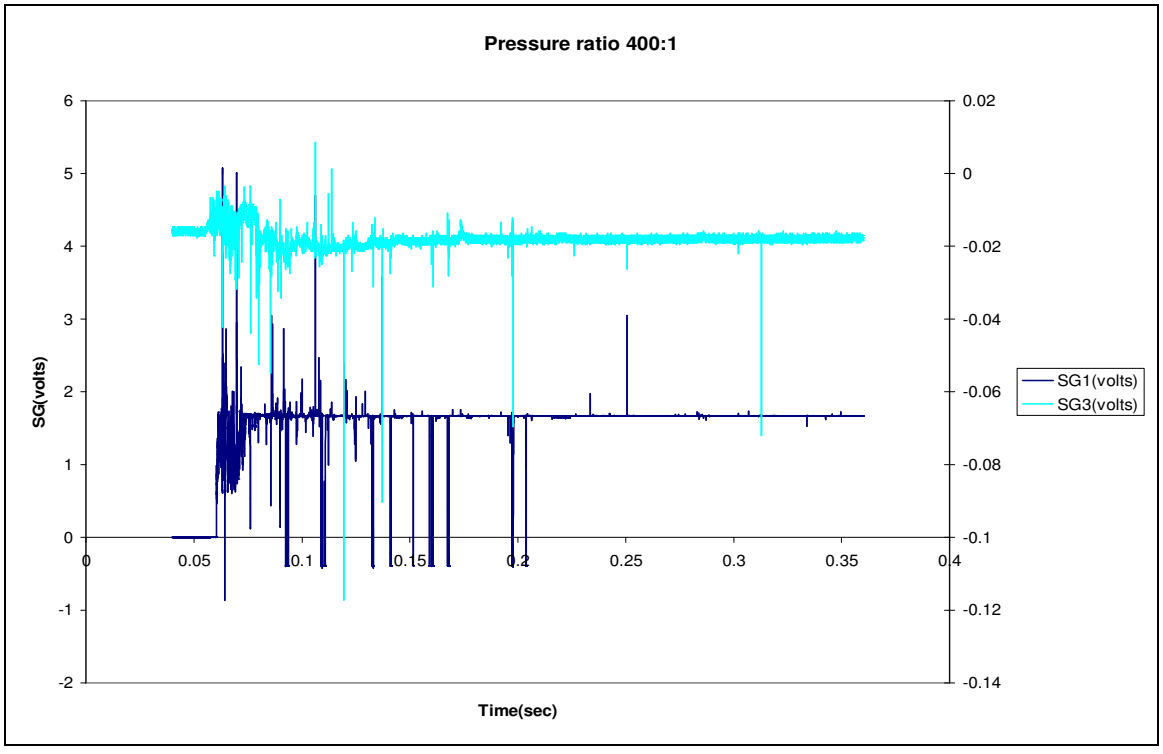

Figure 4.32 Strain gauge plots of Sample 12.

Repeatability is possible if the exact same conditions can be achieved as can been seen from the result of this sample and Sample 8. This will be discussed in the next section. The photograph of the sample is shown below.

Figure 4.33 Sample 12 in the test section after the test.

The cylinder has been pushed forward in the test section proving that the reflected shock is very strong and has damaging effect on the cylinders at higher Mach numbers. As one can see from the strain gauge plots, there is a lot of attenuation in the wave as it passes through the cylinder for lower wave strengths. This was also observed on Sample 8.

4.3 Wave propagation

In this section, the wave propagation through the cylinder at various Mach numbers is studied. This is not a complete study as determination of the instant of wave impact could not be possible due to malfunctioning of gauges resulting in lack of necessary data. The distance between each gauge is 10.16 cm (4 inches). The cylinder is divided into 3 different sectors for calculating the propagation speed through it. The first

sector is 0 to 10.16 cms (0-4 inches) from proximal face, the second sector is 10.16 to 20.32 cms (4-8 inches) from proximal and the last 10.16 cms (4 inches) along the length forms the third sector. The Mach number and the speeds of the wave at the end of each sector through different samples are shown in the following table.

Table 4.2 Mach number and propagation speeds of different samples

Sample	Time of Transducer 1 (sec)	Time of Transducer 2 (sec)	Time of Strain Gauge 1 (sec)	Time of Strain Gauge 2 (sec)	Time of Strain Gauge 3 (sec)	Time of Strain Gauge 4 (sec)	Mach No	Speed of wave in Sector 1 (m/s)	Speed of wave in Sector 2 (m/s)	Speed of wave in Sector 3 (m/s)
1	0.0685	0.0702	0.09002	0.0965	0.1106	0.27	2.37	**15.68**	**7.21**	**0.64**
2	0.06853	0.07017	0.09105	0.09651	0.1057	0.20711	2.46	**18.61**	**11.06**	**1.00**
4	0.01055	0.01205	0.0189	0.02063	0.02507	na	2.69	**58.74**	**22.89**	
5	0.05082	0.05235	0.05841	0.0609	0.06553	0.12167	2.64	**40.81**	**21.95**	**1.81**
6	0.05571	0.0572	0.06298	0.06467	0.06809	0.1193	2.71	**60.13**		**1.98**
7	0.05238	0.05396	0.06717	0.06978	na	0.13334	2.55	**38.94**		
8	0.05126	0.05274	0.06096	0.06256	0.06693	0.11011	2.73	**63.52**	**23.26**	**2.35**
9	0.05203	0.05366	0.06717	na	0.07183	na	2.47			
10	0.05348	0.05508	0.06648	0.06932	0.07481	na	2.52	**35.78**	**18.51**	
11	0.05211	0.05354	0.06026	0.0624	na	0.09175	2.82	**47.49**		
12	0.05133	0.05281	0.06061	na	0.06651	na	2.73			

4.3.1 Variation along the cylinder

It can be seen from the above table that the speed of the wave propagation reduces drastically as it passes through the cylinder. This proves the fact that there is attenuation of the wave as it passes through the cylinder. It can be seen that the wave speed reduces by half by the time it reaches sector 2. Similarly the speed in sector 3 is very low of the order of 10 m/sec.

From sample 8 and sample 12, it can be seen that the time it takes to propagate through the cylinder for the same Mach speed wave is almost same. The time difference in the instants of impact at points 3 and 1 in samples 8 and 12 can be calculated to be .00597 sec and 0.0059 sec respectively. This proves that there is repeatability in the values though it is very difficult to achieve.

4.3.2 Variation with Mach number

The graphs showing the variation of propagation speeds with Mach numbers in the different sectors is shown in Figures 4.34, 4.35 and 4.36.

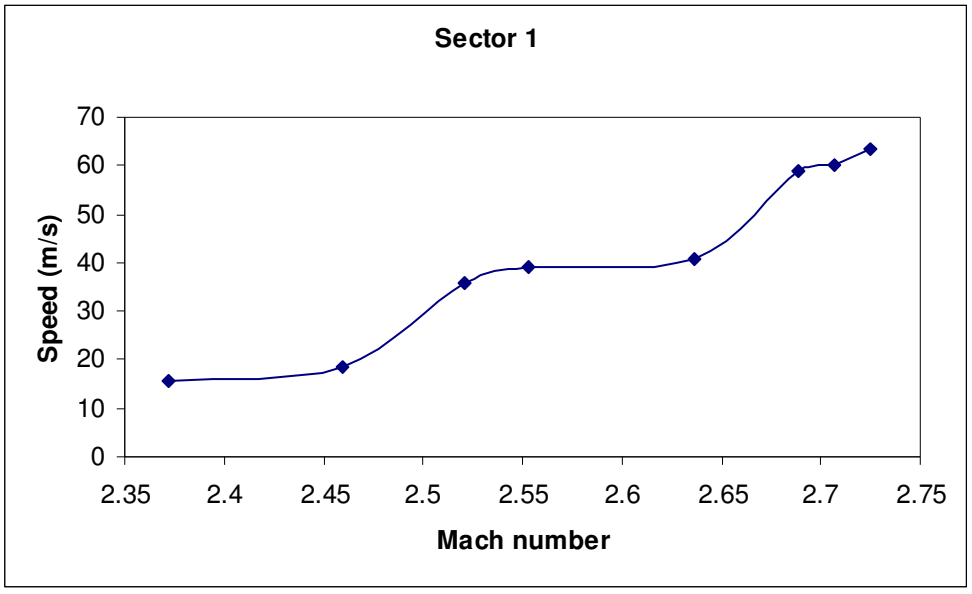

Figure 4.34 Speeds at the end of Sector 1 (line for visual aid only).

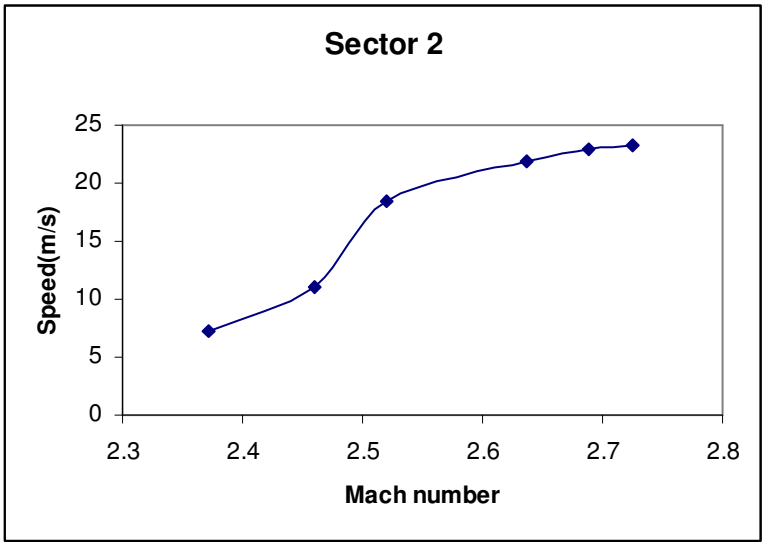

Figure 4.35 Speeds at the end of Sector 2 (line for visual aid only).

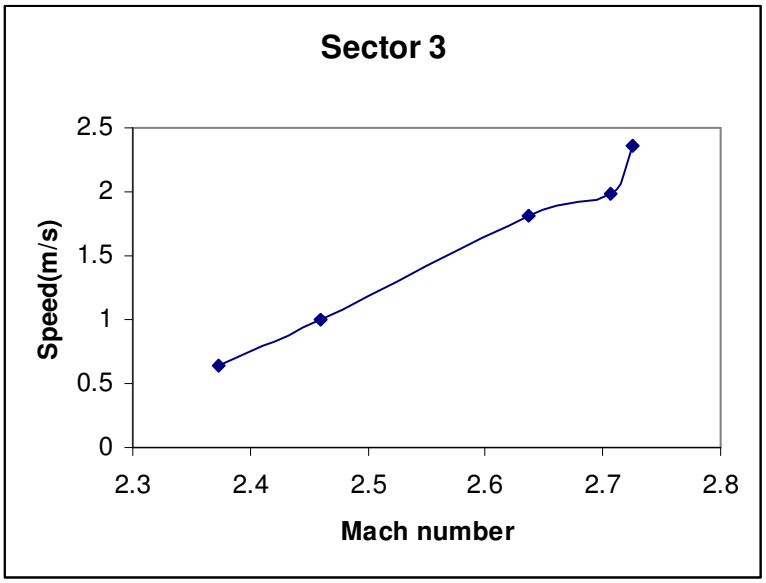

Figure 4.36 Speeds at the end of Sector 3 (line for visual aid only).

The general trend of the wave speeds is that of increasing with Mach number in all the three sectors. The maximum increase in both the sectors can be found between Mach number 2.5 and 2.6 in sector 1 and sector 2 plots. The speed varies the maximum with Mach number in sector 1. This can be attributed to the fact the wave possesses maximum amount of energy as soon as it enters the cylinder. At the end of sector 2 it can be found that the wave speed attenuates to around 20 m/sec after Mach 2.6. This might be a limit for the particular concrete mix of 8 inches thickness. The speed further reduces drastically as it exits the cylinder (end of sector 3). It reduces to around 1- 3 m/sec. Thus a wall of 12 inches thickness can be extremely useful for enduring most blasts in the above range though it may not be very practical.

4.4 Comparison of blast and shock wave pressures

A brief comparison of the different shock waves to its blast wave equivalent is done in this section. This is done by calculating the total pressure of the shock wave based on formulae (2-18) and (2-19) from the Mach number and static pressure ahead of the wave. This total pressure is used to calculate the blast wave parameter called the Z-parameter from (2-21) & (2-23). This Z- parameter determines the strength of a blast in the following terms

$$Z = \frac{R}{W^{1/3}} \tag{4-1}$$

where R is the distance from the charge center in meters and W is the charge mass in kilograms of TNT. These calculations for different samples listed in Table 4.3.

Table 4.3 Z-parameter for various samples

Sample Number	Mach Number	Static pressure ahead of the shock(p1)(psia)	Static pressure behind the shock(p2)(psia)	Total pressure of the shock wave (psia)	Total pressure of the shock wave (kPa)	Z-parameter (± 0.001)
1	2.37	1.147	5.70	79.78	550.1	1.83
2	2.46	1.116	5.94	95.32	657.2	1.668
4	2.69	1.529	9.69	221.80	1529	1.146
5	2.82	1.157	8.05	225.45	1554	1.138
6	2.71	1.34	8.61	202.48	1396	1.189
7	2.55	2.214	12.68	235.12	1621	1.119
8	2.73	1.026	6.68	161.57	1114	1.307
9	2.47	1.059	5.71	93.71	646.1	1.682
10	2.52	1.167	6.52	115.08	793.5	1.521
11	2.82	1.145	7.97	223.11	1538	1.143
12	2.73	1.033	6.72	162.67	1122	1.303

The maximum Z-parameter was 1.83 and minimum Z-parameter was 1.119. A lower parameter represents stronger blast strength. The Z-parameter increases with increase in Mach number. There is a slight variation in the Z- parameter based on the ambient pressure for the same wave speed. Table 4.4 contains the distance from centre of blast for specific masses of TNT at different Z-parameters simulated during our test and vice-versa.

Table 4.4 Ranges and Masses of TNT for various Z-parameters

Z- parameter	W in kg when R=1m	W in kg when R=10 m	R in m when W=1 kg	R in m when W=10 kg
1.119	0.71	713.69	1.12	2.41
1.138	0.68	678.54	1.14	2.45
1.143	0.67	669.67	1.14	2.46
1.146	0.66	664.43	1.15	2.47
1.189	0.59	594.91	1.19	2.56
1.303	0.45	452.03	1.30	2.81
1.307	0.45	447.89	1.31	2.82
1.521	0.28	284.19	1.52	3.28
1.668	0.22	215.48	1.67	3.59
1.682	0.21	210.15	1.68	3.62
1.83	0.16	163.17	1.83	3.94

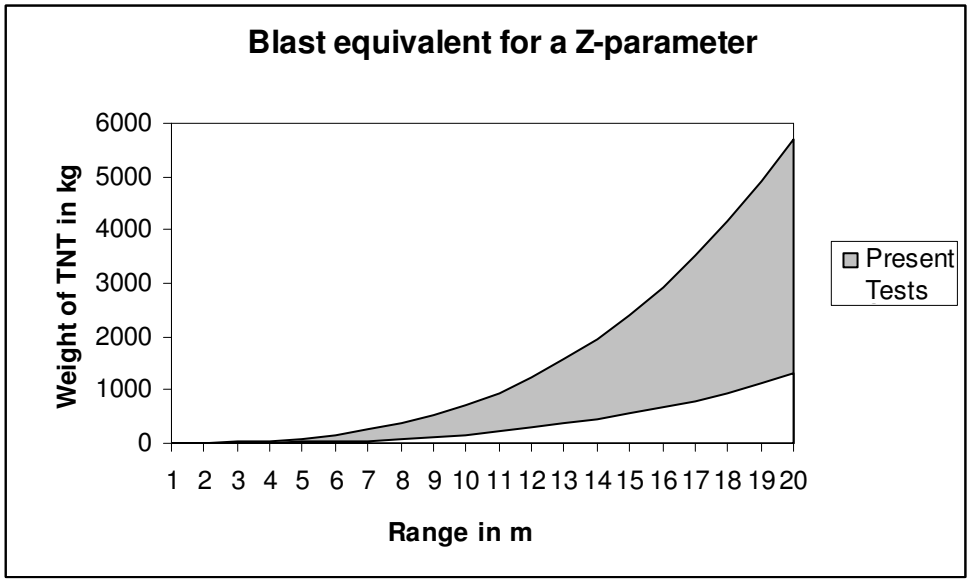

Figure 4.37 Variation of mass of TNT and distance of centre of blast.

Figure 4.37 represents the variation between Mass of TNT and distance from centre of blast for our maximum and minimum Z-parameters. It shows a huge range of blast wave strengths ranging from 1 kg of TNT at a distance of 1 m to 5500 kg of TNT at a distance of 20 m.

4.5 Summary of the Results.

The following are summary of the results:

- Attenuation of blast wave as it passes through the cylinder
- Wave speed in concrete increases with Mach number
- Rate of attenuation increases as the wave passes through the cylinder
- Reflection wave is stronger leading more damage on the proximal side compared to distal side of the cylinder
- The concrete mix is good as a non destructive protection till around Mach 2.5 which corresponds to a Z-parameter of 1.7
- Large ranges of blast wave can be simulated in the shock tunnel
- Strain gauge is not a very effective for study of wave strength in a cylinder

These results shall be discussed in detail with relation to its implementation in protection from blasts in the next chapter.

CHAPTER 5

CONCLUSIONS

Protection of buildings from explosions has been a major safety concern for decades. The experiments conducted on the concrete cylinder have provided us with some data which can be used as preliminary data for consideration while building protection around structures. The major two conclusions discussed in this chapter are the variation of wave propagation through the weak mix suggested and its potential as a material for building protective walls around existing structures. Finally, a few future research possibilities are highlighted.

5.1 Variation of wave propagation

Experiments were conducted on the cylinders by varying the shock Mach numbers which in turn varies the impact stagnation pressure on the cylinders. In all the experiments, it has been found that there is attenuation of wave strength as the shock wave passes through the cylinder. The wave speeds are reduced to $1/5^{th}$ of the speeds in the initial sector of the cylinder by time the wave exits the cylinder. The wave speed reduces by half by the time the wave reaches two thirds of the cylinder length. The weak concrete mix (high percentage of sand) is useful in the attenuation and weakening of the blast wave.

Qualitative examination of the cylinders after the experiments helped us to understand about the physical effects of the wave impact. The cylinders underwent a greater amount of physical damage at higher stagnation pressures (higher shock Mach numbers) compared to lower stagnation pressures. There was more damage on the distal side of the cylinder compared to the proximal side of the cylinder in all the experiments. At high stagnation pressures (Mach numbers greater than 2.7), it was seen that the cylinders were pushed forward and were outside the test section. This proves that the reflecting shock wave is much stronger than the incident blast wave and causes more damage in case of an explosion.

The exit speed of the blast wave from the cylinder increases with increase of incident Mach number. It has also been observed that the exit speed does have an effect on the strength of the reflecting shock wave. In other words, greater the Mach number greater is the strength of the reflecting shock wave on the cylinder. The study of reflecting shock wave could not be done in detail as the strain gauges broke off or became defunct once the incident wave passes through it. Even if the strain gauge is functional, the response of the gauge becomes very unreliable. Therefore a better method has to be employed to study the effect of reflecting shock wave.

Blast waves have been simulated successfully in a controlled environment using shock waves. Though they are different in the pressure variations behind the two waves, their stagnation pressures are constant leading to a correlation between them in terms of the mass of explosive and the distance of the centre of blast. This ratio of these two factors is the Z-parameter used in blast studies. It was also found out that the stagnation

pressure blasts not only depend on the wave speeds but also has a direct variation based on the ambient pressure.

5.2 Protection of structures

The weak concrete mix used in our study can be used to build a secondary wall to protect primary structures from a blast based on certain constraints. The mix is good for protecting buildings from low strength blasts i.e. Z-parameter greater than 1.5 (blast wave speeds of Mach number less than 2.5). At higher blast strengths, the secondary wall gets blown off due to the strong reflecting blast wave. Therefore it should be used only protecting isolated structures with vast spaces around it from blasts which have its centre outside the wall. This mix cannot be used for protecting buildings from high power explosions in crowded cities. Ordinary terrorist attacks are of the Z-parameter range greater than 2 (1 kg TNT @ 2 m or 1000 kg @ 20m). Therefore this can be used to protect ordinary buildings from explosions. Further research has to be done before any conclusions can be made on protection from high power explosions.

5.3 Recommendations for Future work

Different mixes of concrete can be tested to find the optimal mix to provide protection from all blasts. Embedding absorbent materials like foam in concrete or using shape memory alloys for protection are other avenues that can be investigated. Pressure transducers or other methods can be used to do a quantitative study the effect of reflecting wave on concrete. Higher Mach numbers can be studied to study the effect of

nuclear bomb and other powerful blasts. A large number of investigations in different aspects of the blast wave impact has to be made before we can effective conclude on a certain mix and method for building fail safe protection around structures. It is a race against the destructive technology which is developing at a tremendous pace today.

REFERENCES

[1] Committee on Feasibility of Applying Blast-Mitigating Technologies and Design Methodologies from Military Facilities to Civilian Buildings, National Research Council. *Protecting Buildings from Bomb Damage: Transfer of Blast-Effects Mitigation Technologies from Military to Civilian Applications*. National Academic Press, Washington D.C, 1995.

[2] Smith, P.D., & Hetherington, J.G. (1994). *Blast and Ballistic Loading of Structures*. Butterworth-Heinemann, Oxford.

[3] Liepmann, H.W., & Roshko, A. (2001).*Elements of Gas Dynamics*. Dover Publications Inc, New York.

[4] Bourne, N.K., & Stevens, G.S. (2001). "A gas gun for plane and shear loading of inert and explosive targets". *Review of scientific Instruments,* Vol. 72, Number 3, and P.2214-8.

[5] Bourne, N.K. (2003). "A 50 mm bore gas gun for dynamic loading of materials and structures". *Measurement Science and Technology,* Vol. 14, P. 273-8.

[6] Leppanen, J. (2005). "Experiments and Numerical analyses of blast and fragment impacts on concrete." *International Journal of Impact Engineering,* Vol.31, P. 843-60.

[7] Warren, T.L., Fossum, A.F., & Frew, D.J. (2004). "Penetration into low-strength concrete: target characterization and simulations". *International journal of Impact Engineering,* Vol. 30, P. 477-503

[8] Bakken, J., Slungaard, T., Engebresten, T., & Christensen, S.O. (2003). "Attenuation of shock waves by granular filters". *Shock Waves,* Vol. 13, P. 33-40.

[9] Igra, O., Britan, A., Ben-Dor, G., & Shapiro, E. (2004). "Shock wave attenuation by screens and perforated plates." *Symposium on Interdisciplinary Shock Waves Research, Sendai, Japan,* 196-209.

[10] http://encyclopedia.laborlawtalk.com/Shock_wave.

[11] http://www.eng.rpi.edu/mane/lightcraft/Curriculum/Experimental/ShockTube/elements_1.html.

[12] Coleman, H.W., & Steele, W.G. (1989). *Experimentation and Uncertainty Analysis for Engineers*. Wiley Publications, New York.

[13] Stuessy, W.S. (1989). "Hypersonic shock Tunnel Development and Calibration". Masters Thesis, the University of Texas at Arlington.

[14] Emrich, R.J. (1996). "Walker Bleakney and the development of the shock tube at Princeton". *Shock Waves*, Vol. 5, No. 6, P. 327-339.

BIOGRAPHICAL INFORMATION

Ajit Geevarghese John was born on March 3rd, 1981 in Tiruvalla, India, the son of T. G. John and Alice John. He enrolled in Indian Institute of Technology, Chennai, Tamilnadu, India in 1998 and earned his B. Tech. (Bachelor of Technology) in Aerospace Engineering in June 2002.In his senior year, he undertook an internship at the Vikram Sarabhai Space Center in India. He had also worked as a software engineer with Infosys Technologies, India, from August 2002 to August 2003.

Ajit John had started his M.S. (Master of Science) degree in Aerospace Engineering at The University of Texas at Arlington, Arlington, Texas in August 2003 and earned M.S. Degree in Aerospace Engineering in August 2005. During his tenure as a master's student, he was appointed as the Graduate Teaching Assistant of Dr. Frank K. Lu. His thesis was based on the impact of blast waves on concrete surfaces and has wide applications in the protection of structures from the threat of blasts.